

## Chapter 2

# Survival from the Cold Winter: Freezing and Ice Crystallization Inhibition by Antifreeze Proteins

Ning Du, Guoyang William Toh, and Xiang Yang Liu

**Abstract** Antifreeze proteins (AFPs), occurring in some polar animals, plants, fungi, and other organisms, are capable of inhibiting ice freezing at subzero temperatures. The application of AFPs can be found in medicine and industry where low temperature storage is required and ice crystallization is damaging. This includes improved protection of blood platelets and human organs at low temperature, increasing the effectiveness of the destruction of malignant tumors in cryosurgery, and improvement of the smooth texture of frozen foods. In this review, the antifreeze mechanisms of AFPs are discussed, focusing on their inhibition effects on both ice nucleation and crystal growth. AFPs have been found to act in two stages. As a precursor to ice growth, ice nucleation is suppressed by the surface adsorption of AFPs to both ice nucleus and ice nucleators. At the second stage, in cases where inhibition of ice nucleation has had partial or no success, AFPs proceed to inhibit the growth of ice by adsorbing on specific surfaces of ice. Based

---

\*The authors Ning Du, Guoyang William Toh, contributed equally to this work.

N. Du

Department of Physics and Department of Chemistry, Faculty of Science, National University of Singapore, 2 Science Drive 3, 117542, Singapore

Singapore-MIT Alliance for Research and Technology Center, Block S16, 3 Science Drive 2, Singapore, 117543 Singapore

G.W. Toh

Department of Physics and Department of Chemistry, Faculty of Science, National University of Singapore, 2 Science Drive 3, 117542, Singapore

X.Y. Liu (✉)

College of Materials, Xiamen University, 422 Si Ming Nan Road, Xiamen, 361005, P.R. China

Department of Physics and Department of Chemistry, Faculty of Science, National University of Singapore, 2 Science Drive 3, 117542, Singapore

e-mail: [phyluxy@nus.edu.sg](mailto:phyluxy@nus.edu.sg)

on the understanding of structure–activity relationship, one is able to mimic the active domain of AFGPs and synthesize antifreeze glycoproteins by using ligation and polymerization strategies. However, further optimization of the chemistry, as well as new routes to mimic AFPs and functional analogues are needed to allow the routine production of quantities of pure material on commercially relevant scales.

**Keywords** Ice nucleation • Ice crystal growth • Antifreeze protein • Thermal hysteresis • Heterogeneous nucleation • Nucleation kinetics • Ice nucleator • Cryoprotection • Morphological modification • AFP mimics

## 2.1 Introduction

### 2.1.1 *Freezing and Antifreeze in Biological Systems*

Water is the solvent of all biological systems, and the necessity of maintaining a liquid state at the cellular level for life is obvious. For poikilotherms, the limits of cellular function and life are set by the temperatures at which phase transitions of water take place. Thermodynamically, when ice becomes a stable phase, the freezing of water may occur spontaneously. Nevertheless, normally the freezing point of either water or the body fluids of the organism is lower than 0°C due to kinetic factors.

The understanding of the freezing of water in micro-sized water droplets is crucial in climate change, agriculture, food industries, and life sciences [1–5]. Freezing is a process of ice crystallization from supercooled water. In this process, water should undergo the stage of ice nucleation, followed by the growth of ice [6–9]. Nucleation is the key step to determine if or not ice will occur in the supercooled water, while the growth process will determine how big and what shape the ice crystallites will acquire. Actually, whether or not freezing takes place is determined to a large extent by ice nucleation. In other words, there would be no ice crystallization if ice nucleation does not occur. Therefore, to control freezing one should first control ice nucleation and the growth if nucleation control fails.

Due to the fact that ice nucleation is the initial and one of the most important steps in the freezing process, the question of whether ice crystallization is governed by homogeneous or heterogeneous nucleation bears significant implications for antifreeze, ice nucleation promotion, and freezing-related phenomena and activities. It was considered that spontaneous nucleation of ice from water, in particular below –40°C, belongs to “homogeneous nucleation” [2–5, 10, 11]. This implies that the freezing of water is considered to be clean and dusts or foreign bodies exert no influence on nucleation. The key questions to be addressed are whether the conclusion is correct, and if not, under what condition homogeneous nucleation will take place. The latest results indicate that under a well-controlled condition, the influence of dust particles on freezing is still effective below –40°C [12] or heterogeneous nucleation of ice still occurs below –40°C. According to the recent

most accurate estimation of the ice–water interfacial energy, and the homogeneous nucleation barrier, genuine homogeneous ice nucleation may hardly take place even below  $-80^{\circ}\text{C}$  [12]. This implies that if we can eliminate the influence of foreign bodies, freezing may never occur [12].

As freezing is mediated by minute foreign particles, i.e., dust particles, bacterial epiphytes, which cannot be removed completely, in theory, the most effective way to block freezing is to inhibit the promoting effect of foreign bodies on nucleation. In this regard, the understanding of ice nucleation under the influence of minute foreign particles is particularly important for the identification of novel technologies in controlling freezing and antifreeze in general.

Due to the fact that crystallization involves nucleation and growth, the inhibition of the growth of ice crystallites becomes important if the nucleation inhibition fails. We notice that many antifreeze proteins (AFPs) are capable of modifying the growth habit of ice crystallites. As the habit modification is attributed to the retardation of some particular orientations in the crystal growth form [13–17], we therefore can consider the habit modification as a special case of the growth inhibition.

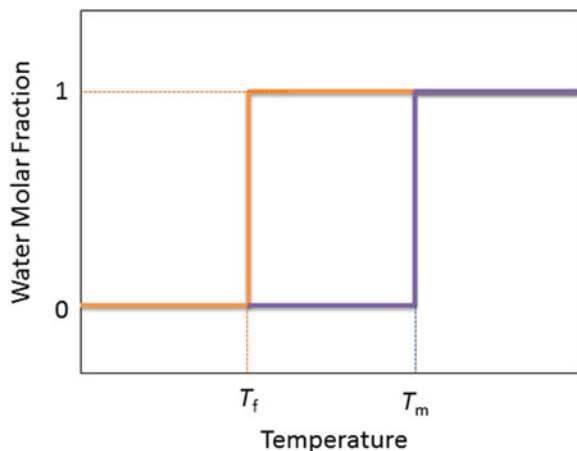
Many plants, fish, insects, and other organisms have evolved with unique adaptive mechanisms that allow them to survive in harsh environments at the extremes of temperature [18–21]. Scholander [22, 23] and DeVries [24, 25] were the first to investigate the mechanisms by which polar fish are able to survive. Analysis of the blood plasma of these fish showed that while the concentrations of salts and small ions in the body fluids are somewhat higher relative to fish in temperate waters, these salts are only responsible for 40–50% of the observed freezing point depression. The remainder of the protective effect was attributed to the presence of a series of relatively high molecular mass glycoproteins and proteins [26–29].

The eminent antifreeze effect results from AFPs found in the blood and tissues of organisms that live in freezing environments [2]. In these organisms, the effect of freezing proteins is retarded, or the damage incurred upon freezing and thawing is reduced [2–4]. Applications of the antifreeze effect of these AFPs, the capacity to inhibit ice crystallization, have been sought for maintaining texture in frozen foods, improving storage of blood, tissues and organs, cryosurgery, and protecting crops from freezing [4].

AFPs and antifreeze glycoproteins (AFGPs) have since been identified in the body fluids of many species of polar fish. The study of annual cycle of AFP production and secretion into the blood in polar fish such as winter flounder indicates that plasma AFP levels correlate closely with the annual cycle of seawater temperatures. AFP appears in the plasma as the water temperature declines, reaches peak levels of 10–15 mg/mL during winter, and clears from the plasma as the temperature rises above  $0^{\circ}\text{C}$  [30]. Peak levels of AFP during winter reduce the plasma freezing temperature of winter flounder to approximately  $-1.7^{\circ}\text{C}$ .

In this chapter, we will review the latest works on freezing kinetics and the antifreeze mechanism of AFP and AFGPs. This includes the effect of a trace amount of foreign nanoparticles on ice nucleation in ultrapure micro-sized water droplets and its implications for freezing and antifreeze in general. As highlighted earlier, how AFPs change the surface characteristics of foreign bodies so as to inhibit ice

**Fig. 2.1** Definition of hysteresis ( $=T_m - T_f$ )



nucleation will be reviewed. The inhibition of AFP and AFGPs on the growth of ice crystals will also be discussed on a surface structural analysis. We notice that although there have been a significant number of papers on AFPs, a comprehensive overview on freezing promotion and antifreeze mechanisms from a kinetic point of view has never been achieved yet. The applications of AFP and AFGPs will also be reviewed at the end. This chapter will provide a platform to review the works in this area. Hopefully, the knowledge obtained here will provide some basic ideas to mimic the antifreeze effect without AFPs.

### 2.1.2 Thermal Hysteresis of AFPs

There are two classes of substances that inhibit water freezing. The first class comprises those solutes that depress both freezing point and melting point. Such substances include sodium chloride, glycerol, glucose, etc. The first class is to change the equilibrium point and can be regarded as a thermodynamic approach. The second class comprises substances having the ability to depress freezing point without significantly affecting the melting point. This is attributed to the change of the freezing kinetics, mainly nucleation and growth. Therefore, the substances mainly block ice formation based on the kinetic factors.

AFPs, also known as thermal hysteresis proteins, lowering the nonequilibrium freezing point of water while not significantly affecting the melting point, belong to the second class. The difference between the freezing and melting points is termed “thermal hysteresis.” The magnitude of this characteristic thermal hysteresis activity is dependent upon the specific activity and concentration of the particular AFP [25] (Fig. 2.1).

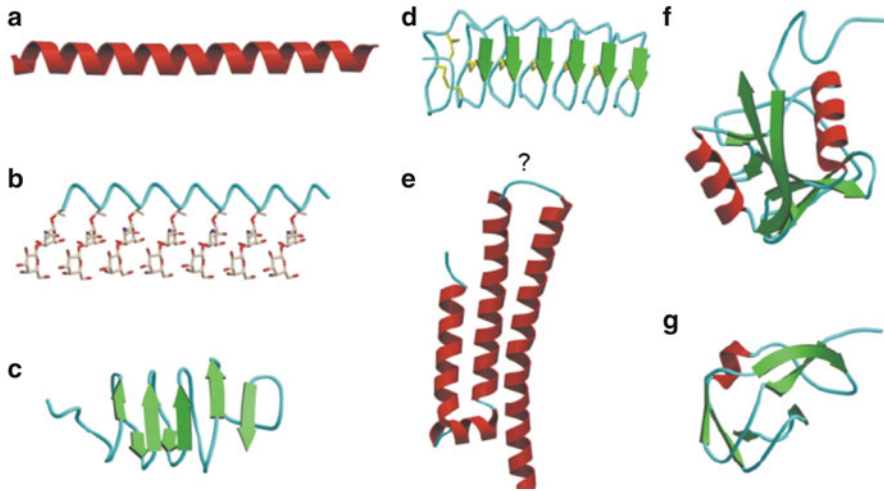


**Fig. 2.2** Diversity of fish AFPs. (a) Type I AFP from winter flounder. (b) Antifreeze glycoprotein (AFGP). (c) Spruce budworm AFP. (d) *Tenebrio molitor* AFP. (e) Type IV AFP. (f, g) Nonrepetitive AFPs. (f) Type II AFP from sea raven (2AFP). (g) Type III AFP from ocean pout. Reprinted with permission from ref. [31]. Copyright (2002) Elsevier

### 2.1.3 AFP Diversity

For over 50 years since their initial discovery, AFPs and AFGPs have been identified in the body fluids of many species of polar fish. Four classes of structurally diverse fish AFPs (cf. Fig. 2.2), classified as type I [32], type II [33], type III [34], and type IV [35], have now been identified along with a single class of glycosylated protein denoted AFGP [36].

Although AFPs were first discovered in fish, the phenomenon of thermal hysteresis was initially observed by Ramsay in larvae of the beetle *Tenebrio molitor* [37] during his classic investigation of the physiology of the cryptonephridial rectal complex. AFPs have also been identified in several other terrestrial arthropods including spiders [38], mites [39], and centipedes [40]. AFPs have been identified, often based on their thermal hysteresis activity, in over 40 species of insects (cf. Fig. 2.2). Among the insects, 65% of the known AFP-producing species are beetles [41]. AFPs have been shown to be also common in plants [42], fungi, and bacteria [19].

## 2.2 Ice Nucleation Inhibition by Antifreeze Proteins

### 2.2.1 Structure of Ice

The crystals of ice consist of a periodic 3D array of water molecules bound together by hydrogen bonds. The hydrogen bonding in water molecules is the starting point to account for the structure of ice. The basic structure of ice is well established by Pauling [43] and illustrated in Fig. 2.3. The oxygen atoms, shown by the dark balls, are arranged on a hexagonal lattice. Hexagonal ice belongs to the space group  $P6_3/mmc$ ,  $a = 4.519 \text{ \AA}$  and  $c = 7.357 \text{ \AA}$ . The unit cell contains four water molecules, taken at the oxygen positions. The O–O bonds, having lengths  $p = 2.763 \text{ \AA}$  and  $q = 2.765 \text{ \AA}$ , are in tetrahedral coordination. Each oxygen has four bonds in the first coordination sphere. Whereas the  $q$  bonds of each oxygen are symmetrically related, the  $p$  bond is symmetrically distinct.

As indicated, in the case of freezing, i.e., ice crystallization, nucleation is the initial and one of the most important steps toward creating ice [1]. Without this step, ice will never occur in supercooled water. In order to discuss the antifreeze mechanism of AFPs, we will first review the nucleation of ice in general.

### 2.2.2 Ice Nucleation Kinetics

Since the nucleation phenomenon was identified and studied by Gibbs, numerous models and theories have been published. Nevertheless, the first detailed experiment monitoring nucleation from the pre-nucleation to post-nucleation stages and quantitatively comparing them with the theories was carried by Liu et al. [45]. A general picture of 3D nucleation was described in ref. [46]. The constituent atoms

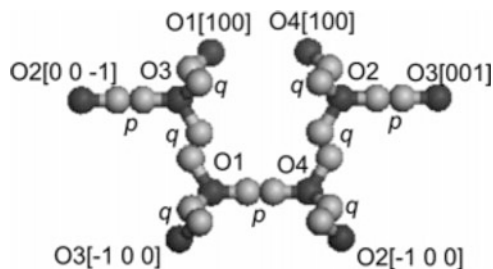


**Fig. 2.3** Unit cell of hexagonal ice consisting of water molecules with oxygen atoms 1–4, projected on a plane perpendicular to the  $b$ -axis, and for each oxygen, the strong bonds ( $p$ ,  $q$ ,  $q$ ,  $q$ ) in the first coordination sphere. Each strong bond consists of two O–O links, mediated by two hydrogen atoms. Dark balls oxygen atoms; light balls hydrogen atoms. Reprinted with permission from ref. [44]. Copyright (2005) American Chemical Society

or molecules in the solution may, on collision, join into groups of two, three, four, or more particles, forming dimers, trimers, tetramers, etc. The kinetics of nucleation is described by the nucleation rate  $J$ , which is defined as the number of nuclei created per unit volume-time, and determined by the nucleation barrier, kink integration rate, transport, and other factors.  $J$  is an important characteristic of the process of new phase formation.

### 2.2.2.1 Thermodynamic Driving Force

Nucleation is the process in which the first-order phase transitions begin. The driving force for nucleation of new phases (e.g., crystals)  $\Delta\mu$ , which is defined as the difference between the chemical potentials of a growth unit in the mother and the crystalline, and for ice crystallization, is given according to [47]:

$$\Delta\mu = \frac{\Delta h_m \Delta T}{T_e}, \quad (2.1)$$

$$\Delta T = (T_e - T), \quad (2.2)$$

where  $\Delta h_m$  is the ice enthalpy of melting per molecule,  $T_e$  is the equilibrium temperature (the melting temperature of ice), and  $\Delta T$  is supercooling.

### 2.2.2.2 Nucleation Barrier

A characteristic feature of the nucleation process is that the substance with the properties of the new phase is fluctuating and localized in small nanoscale spatial regions. These are occupied by various numbers of atoms or molecules in the form of clusters. The clusters remaining at equilibrium with the surrounding mother phase are the critical nuclei, and the smaller or the larger clusters are the subnuclei or supernuclei, respectively. Only the supernuclei are the clusters that can grow spontaneously to reach macroscopic sizes. For simplicity, we call hereafter the subnuclei “clusters,” and the supernuclei “nuclei” (cf. Fig. 2.4a).

The nucleation rate  $J$  describing the number of nuclei successfully generated from the population of clusters per unit time, per unit volume is determined by the height of the free energy barrier, the so-called nucleation barrier. The occurrence of a nucleation barrier is attributed to the following two opposing effects:

1. Since the crystalline phase is a stable phase, the emergence of the new phase from the mother phase will lead to a lowering of the (Gibbs) free energy of the system.

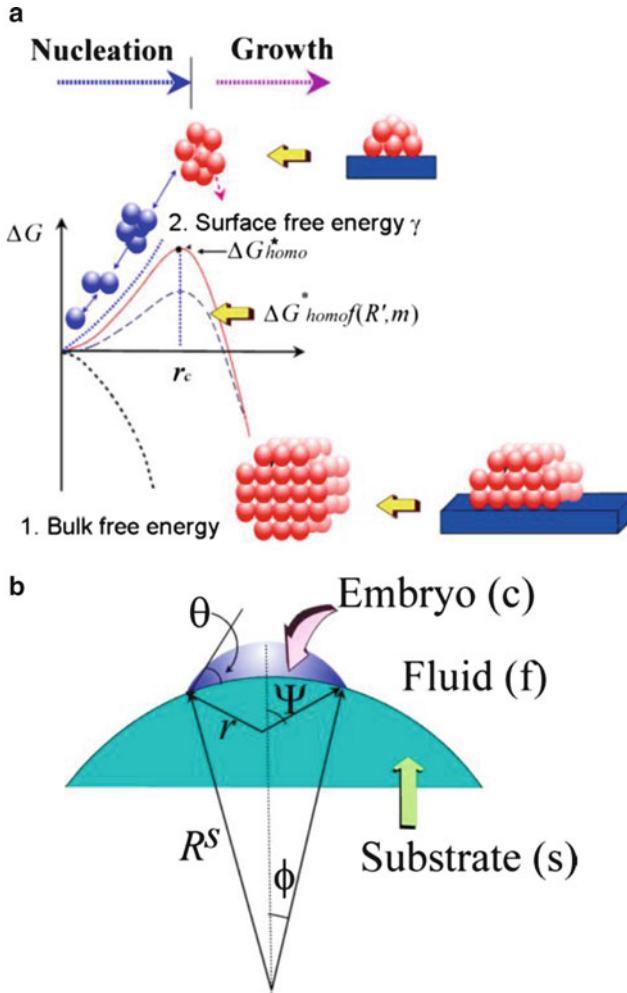


**Fig. 2.4** (a) Crystallization normally takes place via nucleation, followed by the growth of crystals. Nucleation is a kinetic process of overcoming the nucleation barrier, which is the outcome of the occurrence of the surface free energy  $\gamma$ . Reprinted with permission from ref. [48]. Copyright (2012) WILEY-VCH Verlag GmbH. (b) Illustration of nucleation on a foreign particle.  $\theta$  is the virtual contact angle between nucleating phase and substrate. Reprinted with permission from ref. [8]. Copyright (2004) Springer

2. Due to the interfacial (or surface) free energy, the increase in the size of the crystalline new phase leads to an increase in the interface (or surface) area, and consequently the interface (or surface) free energy. This will cause an increase in the Gibbs free energy of the system. The combination of these two effects results in the formation of the nucleation barrier.



The free energy change to form a cluster of  $n = 1, 2, 3, \dots$  molecules can be found by thermodynamic considerations, since it is defined as

$$\Delta G = G_{\text{fin}} - G_{\text{ini}} \quad (2.3)$$

for a system at constant pressure and temperature ( $G_{\text{ini}}$  and  $G_{\text{fin}}$  denotes the Gibbs free energies of the system in the initial and final states before and after the cluster formation, respectively).

$$\Delta G = -n\Delta\mu + \Phi_n, \quad (2.4)$$

where  $\Phi_n$  is the total surface energy of the  $n$ -sized cluster.

$\Delta G$  reaches its maximum  $\Delta G^*$  at  $r = r_c$ , or  $n = n^*$ . The cluster of  $n^*$  molecules is the critical nucleus,  $r_c$  is the radius of curvature of the critical nuclei, and  $\Delta G^*$  is the nucleation barrier. One of the major problems in the nucleation theory is to find  $\Delta G^*$ , which, physically, is the energy barrier of nucleation.

The occurrence of foreign bodies in the nucleation system normally reduces the interfacial (or surface) free energy, which therefore will also lower the nucleation barrier. Under a given condition, if the probability of creating a nucleus is homogeneous throughout the system, the nucleation is considered to be homogeneous nucleation. Otherwise, it is considered to be heterogeneous nucleation. In heterogeneous nucleation on solid or liquid surfaces, microclusters, dusts, and macromolecules, the property of these foreign bodies is an additional factor upon which this barrier and rate depend. Let  $\Delta G_{\text{homo}}^*$  be the homogeneous nucleation barrier, and  $\Delta G_{\text{hetero}}^*$  be the heterogeneous nucleation barrier (the nucleation barrier in the presence of a foreign body.) We can then define here a factor describing the lowering of the nucleation barrier due to the foreign body:

$$f = \frac{\Delta G_{\text{hetero}}^*}{\Delta G_{\text{homo}}^*}. \quad (2.5)$$

In the following,  $\Delta G_{\text{hetero}}^*$  and  $f$  are derived [49].

As shown in Fig. 2.4b, we assume that nucleation occurs at a foreign body with a radius of  $R^s$ . The mother phase is represented by subscript  $f$ , the cluster of the crystalline phase by  $c$ , and the foreign body by  $s$ . If we denote the volume by  $V$  and the surface area of the foreign body by  $S$ , then the free energy of formation of a cluster of radius  $r$  on a nucleating particle of radius  $R^s$  is given, according to (2.4), by

$$\Delta G = -\Delta\mu V_c / \Omega + \gamma_{\text{cf}} S_{\text{cf}} + (\gamma_{\text{sf}} - \gamma_{\text{sc}}) S_{\text{sc}}, \quad (2.6)$$

where  $\gamma_{ij}$  is the surface free energy between phases  $i$  and  $j$  and  $\Omega$  is the volume per structural unit. Assume that the concept of contact angle can still be applied in this case. We have then

$$m = \frac{\gamma_{\text{sf}} - \gamma_{\text{sc}}}{\gamma_{\text{cf}}} \approx \cos \theta \quad (-1 \leq m \leq 1). \quad (2.7)$$

Referring again to Fig. 2.4, we have

$$S_{\text{sc}} = 2\pi(R^s)^2(1 - \cos \varphi), \quad S_{\text{cf}} = 2\pi r^2(1 - \cos \Psi),$$

and 
$$V_c = \frac{1}{3}\pi r^3(2 - 3\cos \Psi + \cos^3 \Psi) - \frac{1}{3}\pi(R^s)^3(2 - 3\cos \varphi + \cos^3 \varphi), \quad (2.8)$$

$$\cos \varphi = (R^s - r \cos \theta)/l = (R^s - rm)/l, \quad (2.9)$$

$$\cos \Psi = -(r - R^s \cos \theta)/l = -(r - R^s m)/l, \quad (2.10)$$

and

$$l = [(R^s)^2 + r^2 - 2R^s rm]^{1/2}. \quad (2.11)$$

To evaluate the critical free energy  $\Delta G_{\text{heter}}^*$ , we can substitute expression (2.8) into (2.6) and require that

$$\frac{\partial \Delta G}{\partial r} = 0. \quad (2.12)$$

Regarding the fact that the radius of curvature  $r_c$  of the critical nuclei is only determined by  $\gamma_{\text{cf}}$  and the driving force  $\Delta\mu$  [49], we then have

$$r_c = \frac{2\Omega\gamma_{\text{cf}}}{\Delta\mu}. \quad (2.13)$$

We notice that in the case of epitaxial growth, some strain will develop due to the structural mismatch at the crystal–substrate interface. The strain will affect both the bulk free energy of nuclei and the interfacial free energy  $\gamma_{\text{cf}}$ . In this case, the occurrence of substrate affects  $r_c$ .

Now substituting expressions (2.7)–(2.13) into (2.6) and writing

$$R' = \frac{R^s}{r_c} = \frac{R^s \Delta\mu}{\Omega\gamma_{\text{cf}}}, \quad (2.14)$$

the free energy of formation of a critical nucleus is

$$\Delta G_{\text{heter}}^* = \Delta G_{\text{homo}}^* f \quad (2.15)$$

with

$$\Delta G_{\text{homo}}^* = \frac{16\pi\gamma_{\text{cf}}^3\Omega^2}{3kS_{\text{m}}^2T\Delta T^2}, \quad (2.16)$$

$$f(m, R') = \frac{1}{2} + \frac{1}{2} \left( \frac{1 - mR'}{w} \right)^2 + \frac{1}{2} R'^3 \left[ 2 - 3 \left( \frac{R' - m}{w} \right) + \left( \frac{R' - m}{w} \right)^2 \right] + \frac{3}{2} m R'^2 \left( \frac{R' - m}{w} - 1 \right) \quad (2.17)$$

and

$$w = (1 + (R')^2 - 2R'm)^{1/2}. \quad (2.18)$$

Here  $R'$  is actually the dimensionless radius of the curvature of the substrate with respect to the radius of the critical nuclei  $r_c$ . In other words, it only makes sense if the curvature of a foreign body or a substrate refers to the curvature of the critical nuclei.

Substituting appropriate values of  $R^s$ ,  $m$ ,  $\gamma_{cf}$ , and  $\Delta\mu$  into (2.13)–(2.18), one can calculate  $f(m, R')$  and  $\Delta G_{\text{heter}}^*$  for any nucleation process. Note that the factor  $f(m, R')$  varies from 1 to 0. Obviously, this factor plays an important role in the determination of the heterogeneous nucleation barrier  $\Delta G_{\text{heter}}^*$ . One can see from (2.5) that the influence of foreign particles on the nucleation barrier can be fully characterized by  $f$ .

Figure 2.5a shows  $f(m, R')$  as a function of  $R'$  for a given  $m$ . When  $R' \rightarrow 0$ ,  $f(m, R') = 1$ , implying that the foreign body as a nucleating substrate will “vanish” completely. In practice, if foreign bodies are too small, i.e., clusters of several molecules, nucleation on these substrates will not be stable. Then, the foreign bodies play no role in lowering the nucleation barrier. If  $R' \gg 1$ , the foreign body can be treated as a flat substrate compared to the critical nuclei. In this case,  $f(m, R')$  is solely a function of  $m$  (Fig. 2.5b), and the curvature of the foreign body has no effect on the nucleation kinetics. Equation (2.17) is then reduced to

$$f(m, R') = f(m) = \frac{1}{4}(2 - 3m + m^3). \quad (2.19)$$

### 2.2.2.3 Heterogeneous Nucleation: The Effect of Ice Nucleators

Let us recapture the picture of the heterogeneous nucleation model. On the substrate surface, some molecular processes occur due to transient visiting molecules that adsorb, form short-lived unions, break up, desorb, etc. An instantaneous census would show some distributions of subcritical nuclei (or clusters) with 1, 2, 3, . . . molecules per cluster (cf. Fig. 2.6). Taking into account the effect of the substrate on both the nucleation barrier and the transport process, and the fact that the average nucleation rate in the fluid phase depends on the density and size of foreign particles present in the system, the nucleation rate is given by [50].

$$J = 4\pi\alpha\beta_{\text{kink}}[(R^s)^2 N^0] f''(m) [f(m)]^{1/2} B \exp[-\kappa f(m)/(T\Delta T^2)] \quad (2.20)$$

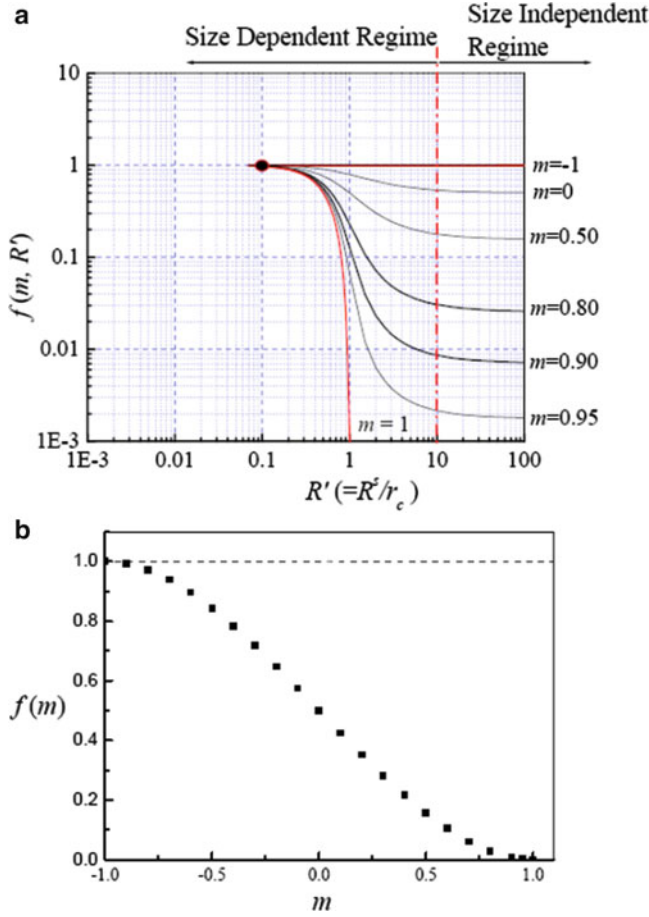


**Fig. 2.5** (a) Dependence of the interfacial correlation function  $f(m, R')$  on  $m$  and  $R'$ . (b) Dependence of the interfacial correlation function  $f(m, R')$  on  $m$  at  $R' > 10$ . Reprinted with permission from ref. [8]. Copyright (2004) Springer

with

$$\kappa = \frac{16\pi\gamma_{cf}^3\Omega^2}{3kS_m^2},$$

$$B = 14\pi a^2\Omega\left(\frac{\gamma_{cf}}{kT}\right)^{1/2}, \quad (2.21)$$

$$f''(m, R') = \frac{1 + (1 - R'm)/w}{2} \quad (2.22)$$

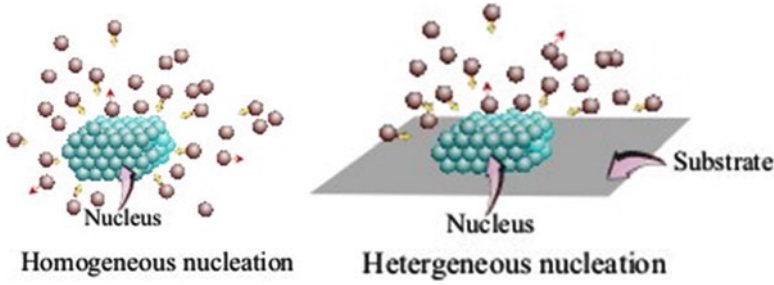


**Fig. 2.6** Scheme of the shadow effect of the substrate in heterogeneous nucleation. Reprinted with permission from ref. [8]. Copyright (2004) Springer

and

$$f''(m, R') = f''(m) = \frac{1}{2}(1 - m) \text{ at } R' \gg 1, \quad (2.23)$$

where  $B$  is the kinetic constant and  $N^0$  denotes the density of substrates (or “seeds”). The growth of nuclei is subject to collisions between growth units and the surfaces of the nuclei, followed by incorporation of the growth units in the nuclei (cf. Fig. 2.6). In the case of homogeneous nucleation, growth units can be incorporated into the nuclei from all directions. However, in the case of heterogeneous nucleation, the presence of substrates will block the collision of growth units with the surfaces of these nuclei.  $f''(m, R')$  in the preexponential term describes the ratio between the average effective collision in the presence of substrates and that of homogeneous nucleation (no substrate).

Both  $f(m, R')$  and  $f''(m, R')$  are functions of  $m$  and  $R'$ . When  $R' \rightarrow 0$  or  $m = -1$ ,  $f(m, R'), f''(m, R') = 1$ . This is equivalent to the case of homogeneous nucleation. In the case where  $m \rightarrow 1$  and  $R \gg 1$ , one has  $f(m, R'), f''(m, R') = 0$ . Normally, heterogeneous nucleation occurs when  $m$  is within the range between 1 and  $-1$ , or  $f(m, R')$  is between 0 and 1, depending on the nature of the substrate surface and supersaturation.

Notice that for homogeneous nucleation, one has  $f''(m, R') = f(m, R') = 1$ , and  $4\pi a(R^s)^2 N^0 \rightarrow 1$ . In this case, (2.20) is converted to:

$$J = B \exp \left[ -\frac{16\pi\gamma_{\text{cf}}^3 \Omega^2}{3kTS_m^2 \Delta T^2} \right]. \quad (2.24)$$

This implies that (2.20) is applicable to describe both homogeneous and heterogeneous nucleation.

One of the most common ways to describe the kinetics of nucleation is to measure the induction time  $t_s$  of nucleation at different supersaturations. By definition, one has

$$J = \frac{1}{t_s V}, \quad (2.25)$$

where  $V$  is the volume of the system. It follows then from (2.20)

$$\ln(t_{\text{nucl}}V) = kf(m)/(T\Delta T^2) + \Delta G_{\text{kink}}^{\#}/kT - \ln(f''(m)(f(m))^{1/2}B') \quad (2.26)$$

with

$$\kappa = 16\pi\gamma_{\text{cf}}^3\Omega^2/3kS_{\text{m}}, \quad (2.27)$$

where  $B' = B[(R^s)^2N^0]$ . For a given system, changes in the slope and/or the intercept of the  $\ln(TV) \sim 1/(T\Delta T^2)$  plot will correspond to the modifications in  $f(m, R')$ ,  $f''(m, R')$  and  $\beta_{\text{kink}}$ .

### “Zero-Sized” Effect of Foreign Particles (Ice Nucleators)

As discussed earlier, the ice nucleation process can be regarded as a kinetic process for ice nuclei to overcome the so-called nucleation barrier  $\Delta G^*$ , under a given supercooling  $\Delta T$  ( $\Delta T = T_{\text{m}} - T$ ;  $T$  and  $T_{\text{m}}$  are the actual and the melting temperatures, respectively). To obtain the ice nucleation kinetics, the correlation between the nucleation induction time  $T$ , the time required for the first nucleus to appear in the drop of water with a given volume  $V$ , and supercooling  $\Delta T$ , was examined. The precise ice nucleation experiments were carried out in a cell based on the “micro water suspending” technology (cf. Fig. 2.7a) [51].

The experiments by Liu et al. [12] show that under normal crystallization conditions, it is almost impossible to eliminate the influence of dust particles. This is evidenced by the fact that the freezing temperature (for a constant droplet volume) decreases progressively as the pore size of the filters is decreased progressively from 200 nm, to 100 nm, to 20 nm (cf. Table 2.1). Actually, in most cases, the term “homogenous ice crystallization,” to which most authors refer [52], is a heterogeneous ice nucleation process promoted by dust particles. This implies that the effect of the dust particles on ice crystallization is inevitable, and should be taken into account in our discussion.

Just as an ice nucleation substrate does, so do foreign bodies always lower the nucleation barrier by a factor  $f$  (cf. (2.15)). For an optimal interaction and structural match between the nucleating phase and the substrate  $m \rightarrow 1$  and  $f(m, R') \rightarrow 0$ , meaning that the nucleation barrier is completely eliminated due to the occurrence of foreign particles. When  $f(m, R') = 1$  (extremely poor structure match/interaction between ice and foreign particles), the nucleation barrier is the highest ( $\sim \Delta G_{\text{homo}}^*$ ) under the given conditions even when the foreign particles are still present, in which case the foreign particles do not play any role in lowering the nucleation barrier.

If freezing were first controlled by heterogeneous nucleation and followed by homogeneous nucleation as  $\Delta T$  increased, we would have obtained for a nucleating system pair-wise intersecting straight-line segments in the  $\ln(\tau V)$  versus  $1/(T\Delta T^2)$  plot (cf. Fig. 2.7b): one segment with a small slope at low  $\Delta T$  (or high  $1/(T\Delta T^2)$ ), the other segment with the largest slope at high  $\Delta T$  (cf. (2.26)). The slope would

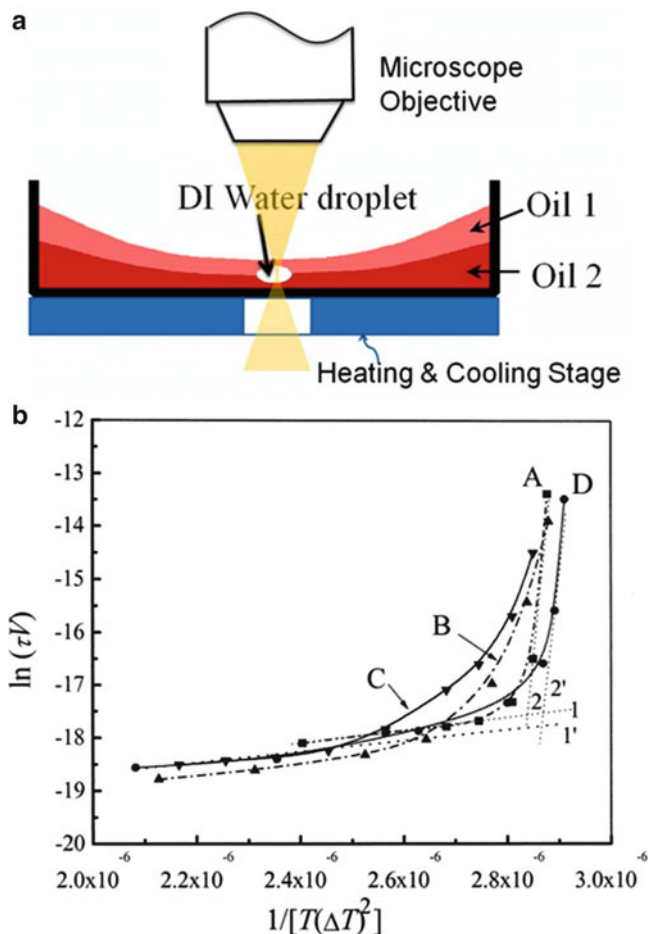


**Fig. 2.7** (a) The “micro water suspending” technology to examine ice nucleation. Illustration of the sample cell and the placement of a microsized DI water drop. The density of Oil I is smaller than water, and the density of Oil II is higher than water. Before experiments, both water and oils were carefully filtrated [51]. (b) The correlation between  $\ln(\tau V)$  and  $1/T(\Delta T)^2$  for DI water filtered by a 20 nm filter (curve A), 0.5 mg/mL AFPIII solution filtered by a 20 nm filter (curve B), 2.5 mg/mL AFPIII solution filtered by a 20 nm filter (curve C), and DI water filtered by a 200 nm filter (curve D). Reprinted with permission from ref. [12]. Copyright (2004) the American Society for Biochemistry and Molecular Biology

then be  $\kappa f(m, R') = \kappa$ , as  $f(m, R')|_{\max} = 1$ ). In contrast to this expectation, we obtain at low  $\Delta T$  (high  $1/(T\Delta T^2)$ ) a straight-line segment with the largest slope within the measurable range of  $\Delta T$ , whereas at high  $\Delta T$  (low  $1/(T\Delta T^2)$ ) we obtain a straight-line segment with a much smaller slope, the two straight-line segments being joined by a curve (Fig. 2.7b). This implies that the nucleation barrier rises abruptly to the highest level ( $\Delta G^* \approx \Delta G_{\text{homo}}^*$ ,  $f(m, R') = 1$ ) at low supercoolings as if the foreign

**Table 2.1** The freezing temperature (for a droplet of constant volume) is dependent on the number and size of dust particles

|                           |     |     |     |
|---------------------------|-----|-----|-----|
| Filter pore size (nm)     | 200 | 100 | 20  |
| Freezing temperature (°C) | −53 | −58 | −65 |

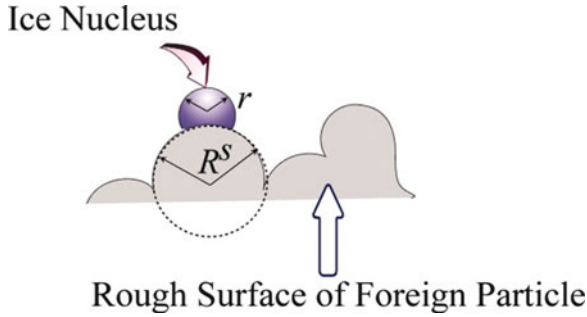


**Fig. 2.8** Illustration of ice nucleation on a rough surface of a foreign (dust) particle. Normally, the surface of dust particles is rough. Therefore, the radius of the local curvature of the foreign particles is smaller than the size of the particles.  $r$ , the radius of the ice nucleus;  $R^s$ , the radius of the local curvature of the foreign particles. Reprinted with permission from ref. [8]. Copyright (2004) Springer

particles had “disappeared” (cf. (2.5) and (2.26)). Notice that the other three curves (B, C, D) share the similar characteristics. Such an effect on nucleation revealed by foreign particles at low supercoolings is called the “zero-sized” effect.

#### Effective Curvature of the Surface Roughness of Foreign Particles (Ice Nucleators)

$R'$  is actually the ratio between the radius of the local curvature of the foreign particles (substrate) and that of the critical nuclei  $r_c$  (2.14, cf. Fig. 2.8).

For a given crystallization system,  $R'$  is proportional to  $\Delta T$  (compare (2.1) and (2.14)). As shown in Fig. 2.5a, the  $f(m, R')$  versus  $R'$  diagram can be divided into three regimes based on  $R'$  or  $\Delta T$ . Regime I (linear regime):  $R' \gg 1$  (relatively large supercoolings and/or large  $R^s$ ). In comparison to the critical nuclei, the foreign particles can be treated as a flat substrate.  $f(m, R')$  then attains its lowest value and becomes a constant with respect to  $R'$  (or  $\Delta T$ ), i.e., it assumes the form  $f(m)$ . According to (2.26), the plot of  $\ln(\tau V)$  versus  $1/(T\Delta T^2)$  is a straight line because  $\kappa$  is constant for a given system (compare portion 1 of curve A in Fig. 2.7b). Regime II (nonlinear regime): as  $\Delta T$  decreases (or  $1/(T\Delta T^2)$  increases),  $r_c$  becomes comparable with  $R^s$  ( $R' \sim 1$ ) (compare (2.14)). The  $\ln(\tau V) \sim 1/(T\Delta T^2)$  plot becomes a curve (compare the curved segment between portions 1 and 2 of curve A) as  $f(m, R')$  varies with  $\Delta T$  (or  $R'$ ). Regime III (zero-sized regime): further lowering  $\Delta T$  (or raising  $1/(T\Delta T^2)$ ) leads to a much larger  $r_c$  than the radius  $R^s$  of the



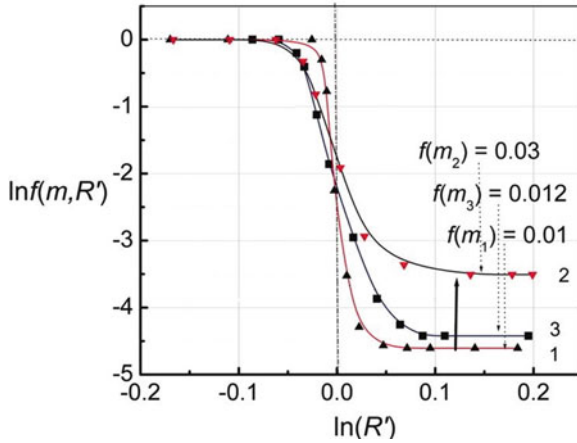


**Fig. 2.9** Experimental  $f(m, R') \sim R'$  for the four different systems: DI water filtered by a 200 nm filter (*curve 1*), 2.5 mg/mL AFPIII DI water solution filtered by a 20 nm filter (*curve 2*), DI water filtered by a 20 nm filter (*curve 3*). The curves were obtained based on the data given in Fig. 2.7b ( $R'$  is obtained based on (2.1) and (2.4)). The entropy of melting per molecule  $\Delta S_m \sim 3.67 \times 10^{-23} \text{ JK}^{-1}$ ; the volume per molecule  $\Omega \sim 32.53 \times 10^{-30} \text{ m}^3$ . Reprinted with permission from ref. [12]. Copyright (2004) the American Society for Biochemistry and Molecular Biology

foreign particles or  $R' \rightarrow 0$ . In the case  $f(m, R')_{\max} = 1$ , one has a straight line with the largest slope (line 2 of curve A in Fig. 2.7b). In this regime, as suggested by the zero-sized effect, the particles behave as if they had “vanished,” although they are still physically present in water. According (2.15), the occurrence of the particles does not lower the nucleation barrier with respect to that of genuine homogeneous nucleation. Notice that the nucleation in Regime III is still not genuine homogeneous nucleation. In the case of genuine homogeneous nucleation, one has  $f''(m, R') = f(m, R') = 1$  and  $\ln(f''(m, R')(f(m, R'))^{1/2} BN^0) = \text{constant}$  for the same system, meaning that only one  $\ln(\tau V)$  versus  $1/(T\Delta T^2)$  plot can be identified in this case for the same system, such as DI water filtrated by a 20 nm filter (Fig. 2.7b, curve A) and DI water filtrated by a 200 nm filter (Fig. 2.7b, curve D). Nevertheless, in comparison to segment 2 in curve A and segment 2' in curve D, one has two parallel straight lines instead of a single straight line. This means that the nucleation occurring at the “zero-sized” regime (Regime III) is still not genuine homogeneous nucleation, although the height of the nucleation barrier is equivalent to that of homogeneous nucleation. This result is attributed to the fact that the probability of nucleation around the foreign particles may still be higher than elsewhere within the water droplet because of the particle-induced molecular preordering. Based on the fact that this homogeneous-like nucleation occurs at low supercoolings rather than at high supercoolings as expected previously [53], this type of nucleation is then referred to as inverse homogeneous-like nucleation.

Figure 2.7b was converted into  $f(m, R') \sim R'$  as given in Fig. 2.9. According to (2.26), the slope of the  $\ln(\tau V) \sim 1/(T\Delta T^2)$  plot is  $\kappa f(m, R')$ . If the inverse

**Table 2.2** The measured transition temperature  $(\Delta T)_{\text{mid}}$  and the radius of the local curvature of foreign particles for different systems

|                                  | $(\Delta T)_{\text{mid}}$ (K) | $(r_c)_{\text{mid}}$ ( $=R^s$ ) (nm) |
|----------------------------------|-------------------------------|--------------------------------------|
| DI water (20 nm filter)          | 39.1                          | 2.28                                 |
| DI water (200 nm filter)         | 33.9                          | 2.54                                 |
| AFP III 2.5 mg/mL (20 nm filter) | 40.3                          | 1.42                                 |

homogeneous-like nucleation takes place (Regime III,  $f(m, R') = 1$ ), one then has  $\kappa f(m, R') = \kappa$ . It follows that the experimental  $f(m, R') \sim \Delta T$  curve can be obtained from the ratio between the slope of the  $\ln(\tau V) \sim 1/T(\Delta T)^2$  plot and the corresponding  $\kappa$  at different  $\Delta T$ . Because  $r_c$  can be obtained from (2.1) and (2.13) and  $\kappa$ , one of the most challenging and important steps in obtaining  $f(m, R') \sim R'$  is to estimate the average local radius  $R^s$  of the rough surface of the foreign particles (compare (2.14) and Fig. 2.7b). As illustrated by Fig. 2.5a (e.g.,  $m = 0.8$ ), one has approximately  $R' \approx 1$  or  $(r_c)_{\text{mid}} \approx R^s$  at the midpoint of the  $\ln(f(m, R')) \sim \ln(R')$  curve ( $-\ln(f(m))/2$ ), enabling one to estimate, according to (2.14),  $R^s$  from  $(r_c)_{\text{mid}}$ , which can be obtained from  $(\Delta T)_{\text{mid}}$  (compare (2.13) and (2.1);  $(\Delta T)_{\text{mid}}$  is the supercooling of the midpoint ( $-\ln(f(m))/2$ ) of the  $\ln(f(m, R')) \sim \ln(\Delta T)$  plot). The values of  $R^s$  for various systems are listed in Table 2.2.

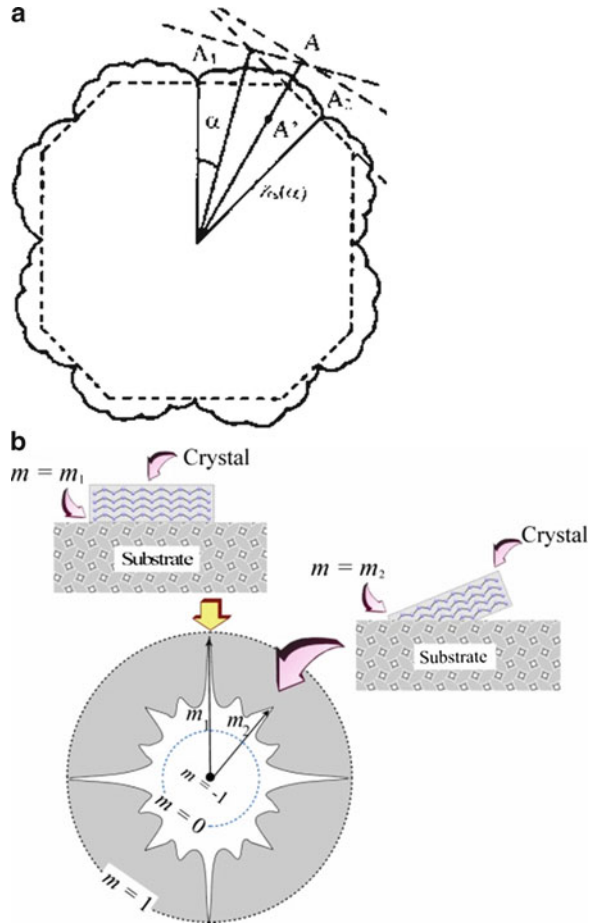
### Interfacial Correlation between Foreign Particles and Nucleating Phase

As shown by Fig. 2.5a, in the case of  $R' \gg 1$ , the substrate can be regarded as being essentially flat, and  $f(m, R')$  is then solely dependent on  $m$ . This implies that  $f(m, R') = f(m)$  is independent of the supersaturation. According to (2.26), the plot of  $\ln(\tau V) \sim 1/(T\Delta T^2)$  should give rise to a straight line whose slope is determined by  $\kappa$  and  $f(m)$ . Obviously, for a given system ( $\kappa, B' = \text{const.}$ ), the slope of the straight line will change according to  $f(m)$ . In this sense, the slope of the  $\ln(\tau V) \sim 1/(T\Delta T^2)$  plot gives the relative  $f(m)$  for the given system. One can analyze the change of the correlation between the substrate and the crystalline phase in terms of the variation of the slope.

As given by (2.7),  $m$  is directly associated with  $\gamma_{\text{cs}}$ , which is determined by the interaction and/or structural match between the crystalline phase and the substrate. For a given crystalline phase and a substrate, an optimal structural match is the crystallographic orientation  $\{hkl\}$ , corresponding to the strongest average interaction or the lowest interfacial energy difference between the crystalline phase and the substrate between the two phases. This orientation corresponds to the (minimal) cusp at the  $\gamma$ -plot (Fig. 2.10a).

As the structural match varies from a perfect to a poor match,  $m$  decreases from 1 to 0,  $-1$ . The extreme case will be  $m \rightarrow -1$ , corresponding to the situation where no crystal–substrate correlation exists. This is the case when substrates exert almost no influence on nucleation, and nucleation is controlled by homogeneous nucleation kinetics. The nuclei emerging in this case are completely disordered, bearing no correlation to the substrate. One has then  $f(m, R') = 1$ .

**Fig. 2.10** (a)  $\gamma_{cs}(\alpha)$  plot in two dimensions. (b) Illustration of  $m$  as a function of crystallographic orientation. The structural match between nucleus and substrate and the corresponding  $m$ . Reprinted with permission from ref. [8]. Copyright (2004) Springer



In general, as  $f(m, R')$  varies from 0 to 1 (or  $m$  from 1 to  $-1$ ), the interfacial structure correlation between the nucleating phase and the substrate changes from a completely correlated and ordered state to a completely uncorrelated and disordered state.

Due to the anisotropy of the crystalline phase, the deviations from the optimal structural match position toward the secondary optimal structural match (the second lowest  $\gamma_{cs}(\alpha)$ , Fig. 2.10b) will adopt discrete values rather than exhibit a continuous change, which is the second lowest minimum of  $\gamma_{cs}$  in the orientation of  $\{h'k'l'\}$ . A similar principle holds for further deviations. Therefore, the deviations from the optimal structural match reflect the transition of  $m$  from  $m_1$  to lower and discrete values  $m = m_2, m_3$ , etc. (cf. Fig. 2.10b).

In the case of nucleation promotion, the adsorption of additives on foreign particles will improve the interaction and/or the structural match between the substrate (foreign particles) and the nucleating phase. This will then result in  $m \rightarrow 1$

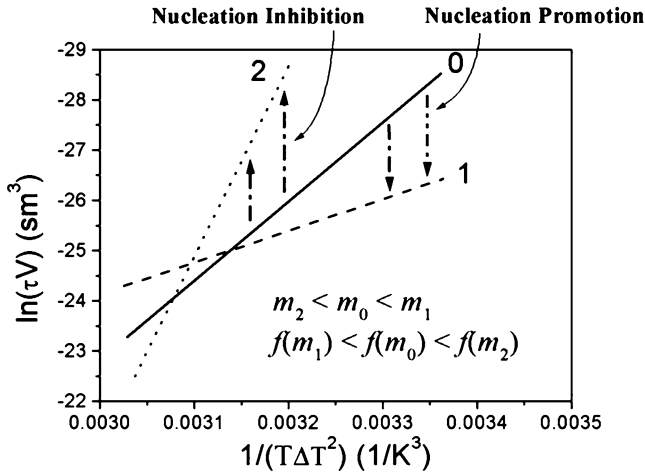


**Fig. 2.11** Illustration of the effect of  $m$  on the nucleation kinetics. The increase of  $m$  will lower the interfacial effect parameter  $f$  and the slope of  $\ln(\tau V) \sim 1/(T\Delta T^2)$  and vice versa. Reprinted with permission from ref. [54]. Copyright (2003) the American Society for Biochemistry and Molecular Biology

and  $f \rightarrow 0$ . Since for a given nucleation system,  $K$  is constant under a given condition (see (2.26) and (2.27)), such a change can then be identified from the lowering of the slope and the increase of the intercept of  $\ln(\tau V) \sim 1/(T\Delta T^2)$  plot (cf. (2.26)). The shift from curve 0 to curve 1 in Fig. 2.11 illustrates this change. Conversely, if the adsorption of additives leads to a stronger repulsion and an interfacial structure mismatch between the substrate and the nucleating phase, one has then  $m \rightarrow -1$  and  $f \rightarrow 1$ . This corresponds to an increase in the nucleation barrier (cf. (2.15)). The effect can be identified from the increase in the slope  $f(m)$  of  $\ln(\tau V) \sim 1/(T\Delta T^2)$  and the decrease of the intercept (from line 0 to line 2 in Fig. 2.11).

#### 2.2.2.4 Surface Kinetics on Ice Nuclei

Apart from overcoming the nucleation barrier, the nucleation of ice is also affected by the incorporation of  $H_2O$  molecules onto the surface of ice nuclei at the kink sites. The rate of kink kinetics is described by  $\beta_{\text{kink}}$ .  $\beta_{\text{kink}}$  is associated with  $\Delta_{\text{kink}}^\#$ , the energy barrier to be overcome in order to remove other molecules adsorbed at the kink sites, and is given by

$$\beta_{\text{kink}} \sim \exp(-\Delta G_{\text{kink}}^\# / kT). \quad (2.28)$$

Obviously, the adsorption of additives on the surface of ice, in particular at the kink sites, will enhance  $\Delta_{\text{kink}}^\#$  by  $\Delta(\Delta G_{\text{kink}}^\#) = \Delta G_{\text{kink}}^{\#'} - \Delta G_{\text{kink}}^\#$ .  $\Delta G_{\text{kink}}^{\#'}$  denotes the kink kinetics barrier attributed to the adsorption of impurities/additives on the

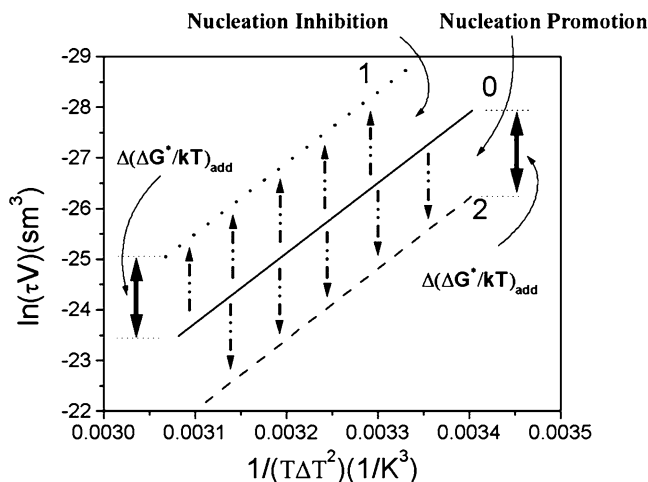


**Fig. 2.12** Illustration of the change in kink kinetics and the corresponding shift in the  $\ln(\tau V) \sim 1/(T\Delta T^2)$  plot. The change in the kink kinetic coefficient  $\beta_{\text{kink}}$  or the kink integration barrier will cause a parallel shift upward or downward, depending on whether there is nucleation inhibition or promotion. Reprinted with permission from ref. [54]. Copyright (2003) the American Society for Biochemistry and Molecular Biology

surface (cf. Fig. 2.12). Consequently, the integration of  $\text{H}_2\text{O}$  units in the ice crystal structure will be significantly slowed down or even stopped due to a very low  $\beta_{\text{kink}}$  (or high  $\Delta G_{\text{kink}}^\#$ ) (cf. (2.28)).

It follows from (2.26) that for ice nucleation, the plot  $\ln(\tau V) \sim 1/(T\Delta T^2)$  will give rise to a straight line for a given  $f(m)$  (and  $f''(m)$ ). The slope and intercept of the line can be utilized to derive the key parameters associated with the kinetics of ice nucleation.

### 2.2.3 Ice Nucleation Inhibition by AFPs

As mentioned earlier, the adsorption of AFP III on the ice nucleators and the impact on nucleation can be quantified from the  $\ln(\tau V) \sim 1/(T\Delta T^2)$  plot. The plots obtained in the aforementioned experiments, using the plots of deionized (DI) water without and with AFP III are given in Fig. 2.13. The slopes and intercepts resulting from the linear regression for these systems are listed in Table 2.3. It follows that ice nucleation is inhibited by AFP III (longer induction time) at the two concentrations. The two effects can be quantified by the changes in the slopes and the intercepts compared with the DI water within the range of supercoolings.

The adsorption of AFP III molecules on ice nucleators turns out to strongly disturb the structural match between the nucleating ice and the dust particles (cf. Fig. 2.13 and Table 2.3). This can be identified from the variation of  $m$  (or  $f(m)$ ),

**Fig. 2.13** The effect of AFP III on the ice nucleation kinetics and the corresponding shift in the  $\ln(\tau V) \sim 1/(T\Delta T^2)$  plot. Reprinted with permission from ref. [54]. Copyright (2003) the American Society for Biochemistry and Molecular Biology

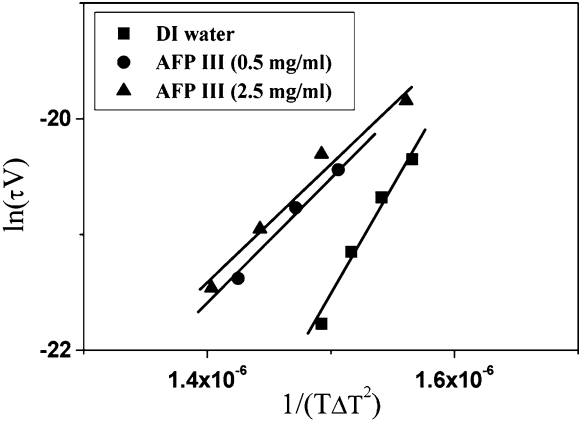


**Table 2.3** Effect of AFP III on the interfacial effect parameter and kink kinetic energy barrier for the nucleation of ice

| Curve                 | $\kappa$           | $f(m)$ | $\Delta G^*/\Delta G_{\text{DIwater}}^*$ <sup>a</sup> | $m$  | $\Delta(\Delta G_{\text{kink}}^\# / kT)_{\text{add}}$ |
|-----------------------|--------------------|--------|---|------|---|
| DI water <sup>b</sup> | $1.21 \times 10^8$ | 0.2    | 1   | 0.43 | –   |
| AFP III(0.5 mg/mL)    | $0.39 \times 10^8$ | 0.35   | 1.75  | 0.20 | ↑ 13.7  |
| AFP III(2.5 mg/mL)    | $0.32 \times 10^8$ | 0.45   | 2.25  | 0.07 | ↑ 13.9  |

<sup>a</sup>  $\Delta G^*/\Delta G_{\text{DIwater}}^* = f(m)_{\text{AFP III}}/f(m)_{\text{DIwater}}$  <sup>b</sup> DI water: deionized water

which decreases from 0.43 to 0.2 and 0.07 and the enhancement of the nucleation barrier by a factor 1.75 and 2.25, for a 0.05 wt% and 0.25 wt% solution, respectively.

The results given in Fig. 2.13 and Table 2.3 show that AFP III will also adsorb onto the growing ice nuclei. This can be seen from the increase in the desolvation kink kinetics barrier  $\Delta G_{\text{kink}}^\#$  (13.7kT for 0.05 wt% solution, 13.9kT for 0.25 wt% solution, cf. Table 2.3).

It is worth noting that the presence of the AFP III molecules on the surface of the embryos causes the interfacial free energy  $\gamma_{cf}$  between the crystalline phase c and mother phase f to decrease. Based on (2.27), this change will lower  $\kappa$  and induce nucleation promotion. However, the aforementioned analysis shows that this promotion effect is not dominant compared to the other two inhibition effects of AFP III.

### 2.3 Ice Crystal Growth Inhibition by Antifreeze Proteins

#### 2.3.1 Ice Crystal Growth Inhibition

As ice crystallization includes both nucleation and growth, once the inhibition of ice nucleation fails, AFPs should proceed to inhibit the growth of ice.

The growth of crystals occurs at the boundaries/interfaces between the crystal phase and the fluid phase when the boundaries move toward the fluid phase. In this sense, the configuration of crystal surfaces will to a large extent determine the growth kinetics of crystal faces [55–68]. We normally have two types of crystal surfaces: the surfaces with an essentially flat configuration—*so-called flat crystal surfaces*, or with a rough configuration—*so-called roughened crystal surfaces* (Fig. 2.14a). The growth of crystals will therefore be in one of the two modes: (1) faceted growth or layer-by-layer growth mode or (2) roughened growth or normal growth mode, respectively [60–65]. A faceted crystal surface will have a transition from the flat mode to the rough mode at the temperature higher than the critical temperature, so-called roughening temperature  $T^R$  [55–58, 66].

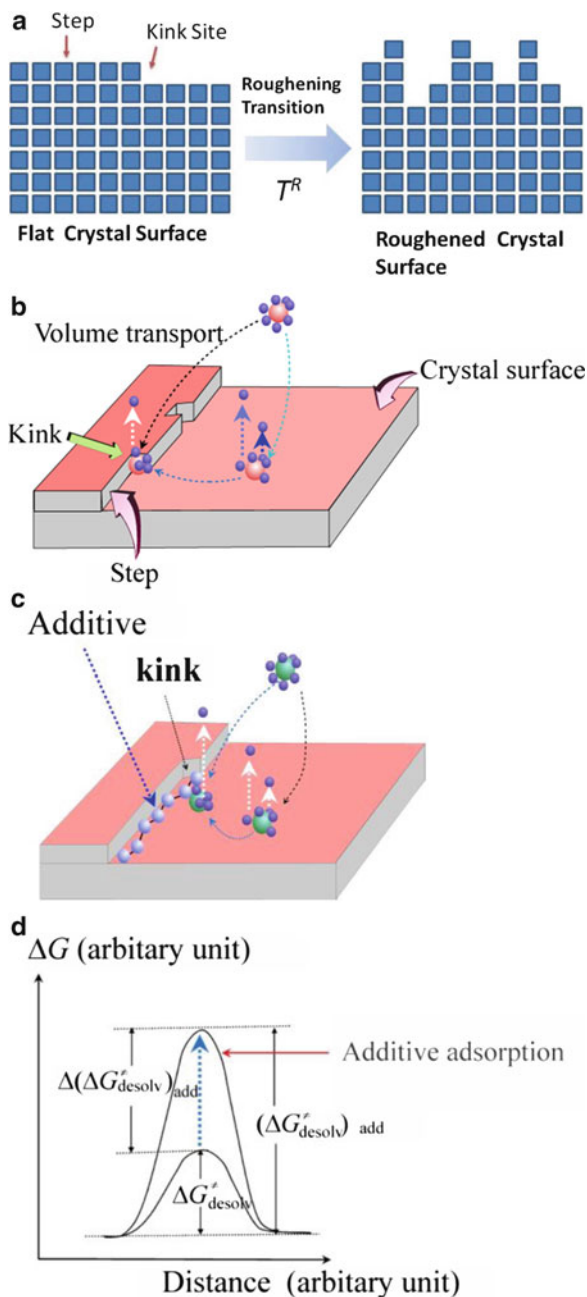
In general, the growth of crystals can be regarded as a process of delivering growth units from the bulk to the crystal surface and incorporating these units into the kinks (cf. Fig. 2.14b). In the case of faceted growth, the crystal face is atomically smooth and the kinks occur only at the steps. In this case, the steps can be regarded as “sinks” for growth units to enter the crystals [8]. As shown in Fig. 2.14b, each advancing step will disappear when it spreads over the surface and reaches the edge of the surface. In order to continue the growth of the crystal surface, a subsequent crystal layer needs to be generated on the existing crystal surface. Therefore, the step source for the creation of new layers will determine the growth rate of the crystal surface. Due to the presence of a step free energy, the creation of a new layer on the existing layer of the crystal surface requires overcoming that free energy barrier, which is the so-called 2D nucleation barrier [67]. Normally, for the growth of flat or faceted crystal surfaces, the screw dislocations occurring on the surface will provide uninterrupted step sources for a layer-by-layer growth [68], and in such cases the growth is controlled by screw dislocation mechanisms [68].

The growth of crystals that are free from screw dislocations is governed by the so-called 2D nucleation growth mechanism [67]. This implies that the crystal faces grow by depositing one crystal layer on top of the previous layer [67].

Ice crystal growth inhibition is attained by reduction of the growth rates of all crystal faces occurring on the ice crystallites. One of the mechanisms is to “pin” the growing steps by adsorbing additive (i.e., AFPs) molecules onto the surfaces (cf. Fig. 2.14c). This happens only when the crystal surfaces are flat. The basic mechanism is that when the average distance between the molecules is smaller than  $2r_c^{2D}$  ( $r_c^{2D}$ : critical radius of 2D nucleation [67]), the movement of the steps on the crystal surface will be blocked. Another mechanism is that the additives are adsorbed at the kink sites so that the kink desolvation free energy barrier is greatly enhanced (cf. Fig. 2.14d). Based on (2.30), the kink integration coefficient  $\beta_{\text{kink}}$  will be significantly reduced [61, 62]. The second mechanism is applied to both flat and rough crystal surfaces.

Note that a substantial curtailment of the growth of ice would amount to a substantial reduction of the absolute size of the ice crystallites. This is a commonly occurring phenomenon, as evidenced by the relatively small sizes of the ice crystals found in the bellies of fish in subzero environments. If all facets are inhibited by

**Fig. 2.14** (a) Schematic illustration of flat and roughened crystal surfaces [55–58, 66]. Normally, flat crystal surfaces will grow slower than roughened crystal surfaces and dominate the crystal morphology. (b) Schematic illustration of the surface integration occurring on the surface of a cluster. Reproduced with permission from ref. [69]. Copyright (2001) American Chemical Society. (c) Schematic illustration of the adsorption of additives at a kink site and (d) the enhancement of the kink desolvation free energy barrier. Reprinted with permission from ref. [8]. Copyright (2004) Springer





equal proportions, then the crystallites will be smaller but will retain the same shape; however, preferential inhibition of some surfaces over others will lead to both smaller crystallites and a modified shape. In this section, the AFP-induced ice morphological modification is discussed, focusing on a comparison of various ice morphologies produced by different types of AFPs.

### 2.3.2 AFP-Induced Morphological Modification

Crystals, including ice crystals, are bounded by the faces of the lowest growth rate. Therefore, the morphology of crystals is determined by these crystal faces. In general, crystals are bounded by faceted faces as these are the slow growth faces. For a given crystalline material, i.e., ice, if the ratio of the growth rates of these faces remains unchanged, the morphology of the crystals will be identical. Nevertheless, once the growth rates of some particular surfaces are reduced due to the selective adsorption of additives (i.e., AFPs or AFGPs), the shape or morphology of crystals will be modified (cf. Fig. 2.15).

Given a crystal system, the prediction of the growth morphology of crystals is equivalent to the prediction of relative growth rate in different crystallographic orientations. The primary surfaces can be used to derive the structural morphology [70–72]. The simplest one is the Bravais–Friedel–Donnay–Harker law [73]. Whether or not a primary surface will actually appear on the growth form, and to what extent it will dominate the morphology, depends on the relative growth rates of the neighboring surfaces. According to the BFDH theory, the relative growth rate of the crystal face ( $hkl$ )  $R_{hkl}$  can be predicted by

$$R_{hkl} \propto \frac{1}{d_{hkl}}, \quad (2.29)$$

where  $d_{hkl}$  denotes the lattice spacing of ( $hkl$ ) corrected by the extension condition (cf. Fig. 2.16). The physics consideration of this model is that the interaction between the growth units in the adjacent lattice planes will decrease with the

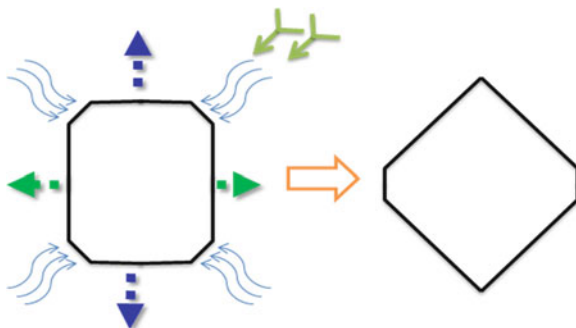


**Fig. 2.15** Illustration of crystal growth habit modification

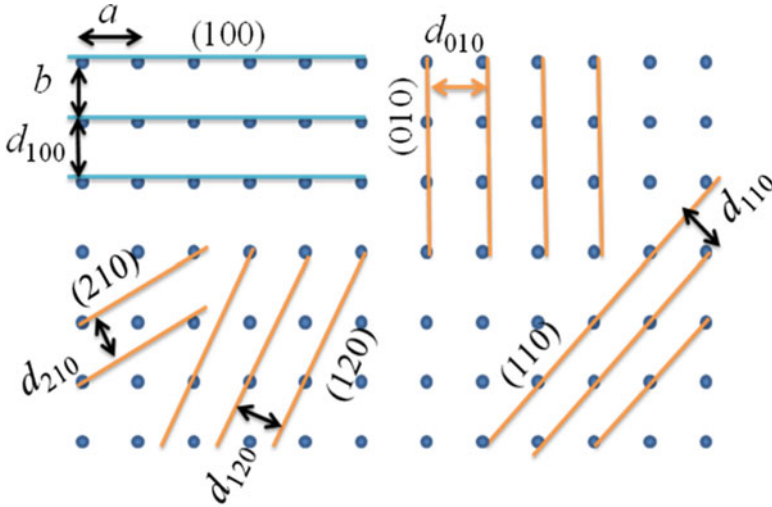


**Fig. 2.16** An orthorhombic lattice projected along the  $c$  axis. The projections of (100), (010), (110), (120), and (210) lattice plans and the corresponding spacings

increase of the spacing. Then the growth rate in the same orientation will decrease correspondingly.

The structure of the morphology of crystals can be plotted by the Gubbs-Wulff plot [13] based on (2.29) and the symmetry of the crystals.

One of the most popular theories is the Hartman–Perdok theory or the periodic bond chain (PBC) theory, which was first published by Hartman and Perdok [13, 74–77]. The key points of the PBC theory can be summarized as follows:

1. In a crystal structure, one can always identify some *uninterrupted* periodic *strong* bond chains (PBCs), running through the crystal structure.
2. A PBC along the direction of  $[uvw]$  should have the basic crystallographic period in the given direction.
3. If one PBC period consists of different types of bonds, the strength of PBC will be determined by the weakest bond.
4. The important crystallographic directions must be in line with the strong PBCs.

An example of PBC analysis is given by Fig. 2.17. In the bond structure given, three PBCs can be identified:  $\text{PBC}[uvw]$ ,  $\text{PBC}[u_1v_1w_1]$ ,  $\text{PBC}[u_2v_2w_2]$ . If the rank of the bond strength is given as strong bond 1 > strong bond 2  $\gg$  weak bond 1 > weak bond 2, one has then  $\text{PBC}[uvw] > \text{PBC}[u_1v_1w_1] > \text{PBC}[u_2v_2w_2]$ .

Based on the concept of PBC, the crystal faces can be classified into three types: F-face, S-face, and K-face (cf. Fig. 2.18).

- F-face: Flat face—more than two nonparallel PBCs in parallel to the surface are identified.

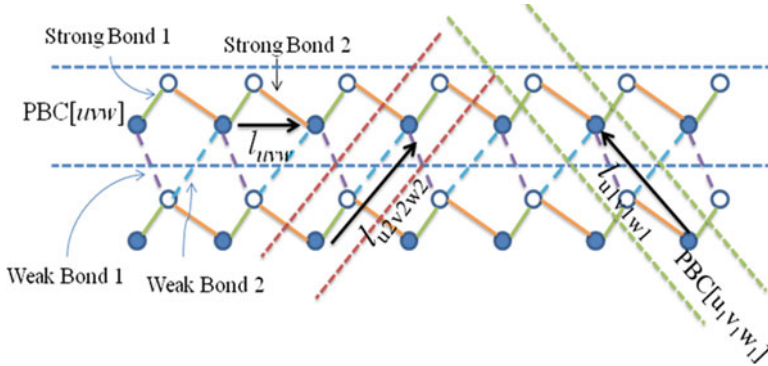
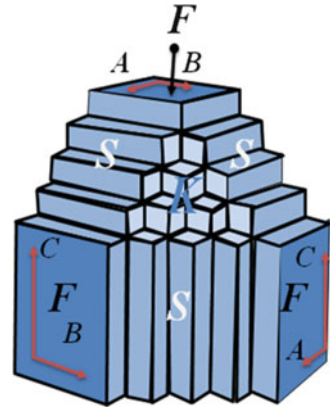


**Fig. 2.17** A crystal bond network and the identification of three PBCs

**Fig. 2.18** Illustration of F, S, and K faces of crystals [74–77]



- S-face: Stepped face (roughened face)—one PBC in parallel to the surface is identified.
- K-face: Kink face (roughened face)—no PBC in parallel to the surface is identified.

According to Hartman [74–77], crystals are bounded by F faces. Here, F faces correspond to the faceted or flat faces while S and K faces are the roughened faces. According to definition of F face, there should be an *interconnected* bond network parallel to an F face (cf. Fig. 2.17). It follows from the modern statistic physics [78] that there will be a nonzero roughening temperature. For S and K faces, since no *connected* bond network occurs in parallel to the faces, the faces are roughened all the time. In summary, the PBC analysis includes the following key steps:

1. Calculate/identify various bonds/interactions connecting the neighboring structural units. (Only the bonds established in the crystallization will be considered.)
2. Identify the bond structure of the crystals.
3. Identify PBCs and the networks in all directions.
4. Identify F faces.

In corresponding to the Bravais–Friedel–Donnay–Harker law, in the Hartman–Perdok theory, the growth rate of F-faces is taken proportional to the attachment energy  $E_{\text{att}}$

$$R_{hkl} \propto E_{hkl}^{\text{att}}, \quad (2.30)$$

$$E_{\text{latt}} = E_{hkl}^{\text{att}} + E_{hkl}^{\text{slice}}, \quad (2.31)$$

where  $E_{\text{latt}}$  denotes the lattice energy of crystals,  $E_{hkl}^{\text{slice}}$  is the slice energy or 2D lattice energy of face  $(hkl)$ . The slice energy refers to the amount of energy contained in that growth layer and  $E_{\text{att}}$ , the attachment energy, refers to the quantity of energy released when a new growth layer becomes attached to the crystal. According to (2.30), the most favorable molecular composition of a primary surface is the one with the smallest attachment energy [70–72]. The implication of (2.30) and (2.31) is that the larger the slice energy (equivalent to smaller attachment energy), the smaller the growth rate and the more crucial the face [71, 72].

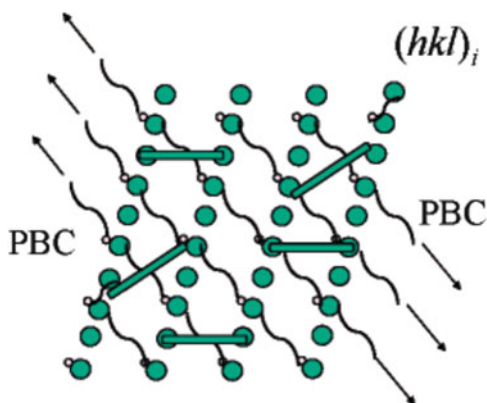
The PBC theory precisely identified the mechanisms by which AFPs alter the ice morphology as reported by Strom et al. [44, 79, 80]. These works overcome the drawback of most other studies in which randomly obtained planar cut surfaces are selected. In fact, crystallographically valid flat surfaces need not be planar cut slices of the structure. Both the AFP–ice interaction and the molecular equilibrium distribution in the AFP–ice–water system depend crucially on the detailed definition of the simulated ice crystal substrates.

The morphological modification caused by external factors can be assessed from knowledge of the growth conditions, that is, usually the surrounding liquid, often containing influential molecular species. Such species may exert an even stronger morphological effect than the liquid itself, as is the case with the AFP (cf. Fig. 2.15).

The slice energies of the low index  $(hk0)$  and  $(h0l)$  secondary surfaces are characterized by relatively high slice energies, comparable to those of the primary surfaces. The main impediment to the appearance of some secondary prismatic and pyramidal facets on the growth form of ice would not likely arise from a modest deficit in the energy of the surface bonding pattern. That impediment is rather due to the lack of bonding in a second lattice direction transverse to the single existing one.

As mentioned before, crystals are only bounded by F faces, not by S or K faces. It is surprising to see some S faces can occur on the morphology of ice crystals when some AFPs and AFGPs are added [31]. It was found that these AFPs and AFGPs can turn the S faces into pseudo “F” faces surface bridging. According to the work by Strom et al. [44], the fish-type ice binding surface stabilizes a secondary surface by introducing effectively a second strong-bonding direction to intersect with the existing one. This is schematically illustrated in Fig. 2.18. Some of the surface molecular compositions available for engagement will offer a better match than others to the ice binding surface structure. The selection of the face indices of the reconstructed surface occurs by identifying the particular surface molecular composition that offers the best structural match or the strongest interaction with

**Fig. 2.19** Schematic illustration of a statistical distribution of fish-type ice binding surfaces on a low-index secondary surface, inducing a surface-reconstruction-type effect while selecting the face indices  $(hkl)_i$ . Reprinted with permission from ref. [44]. Copyright (2005) American Chemical Society



a fish-type ice binding surface. By providing supplementary bonding in various directions transverse to the existing strong bonding direction, the ice binding surface modifies the surface orientation. Out of the numerous possibilities available for the surface orientations parallel to the PBC, the specific face indices  $(hkl)_i$  are selected in Fig. 2.19. Therefore, the indices of the observed ice facets are expected to vary according to the specific properties of the ice binding surface of the AFP and according to the changes in the ice binding surface caused by the experimental conditions.

The available experimental results show that the morphological modification mechanism of surface reconstruction is triggered by two variants of the fish-type ice binding surface. The “one-dimensional” ice binding surface variant found in fish-type I AFPs and AFGPs is characterized by one or more linearly extended helices, having regularly spaced binding intervals in only one direction. It can align its helix/helices along any one of several alternative lattice translations transverse to the existing strong bonding direction, thus mimicking a second intersecting strong bonding direction that is absent from the crystal structure. The bridged distances are lattice periods between adjacent parallel PBCs. Therefore, surface reconstruction through “supplementary *interchain* bonding” is triggered by the 1D ice binding surface variant. In globular type II and III AFPs, however, the “irregular” ice binding surface variant consists of mixed  $\alpha$  and  $\beta$  structures that are not 1D. It need not either be planar or exhibit any spacing regularity in its binding sites in order to function. It can align itself along numerous shorter distances in various directions. It bridges intermolecular distances that need not be lattice translations, by linking oxygen–oxygen pairs on adjacent parallel PBCs. So the irregular ice binding surface variant can trigger surface reconstruction through “supplementary *intermolecular* bonding.”

It has been noted [44] that the geometrical differences between prismatic and pyramidal faces become significant in comparing theoretical prediction against experimental observation. The prism is an open form, implying that it can appear on the crystal habit in combination with other forms but not by itself, for example,

basal plane and/or pyramid. A hexagonal prism seen in isolation cannot be distinguished from another differently oriented hexagonal prism. In contrast, a hexagonal bipyramid is a closed form that can appear on the growth form by itself; however, it can also appear in combination with the basal face and/or various prisms. Visual inspections of the crystallite shape using the height-to-baseline ratio or the apical angle can readily distinguish bipyramids from other differently oriented bipyramids. For that reason, the broad range within which the experimentally observed pyramidal facets differ is directly observable on the obtained images reported in the literature.

Strom et al. [44] have noticed that the fish-type ice binding surface enhances the growth rate along the [001] direction, which is part of the secondary prismatic surfaces ( $hk0$ ). Their face indices, as observed experimentally [81–84], vary from (110) up to (410); (110) is the most frequently reported secondary prismatic form. The identification of the (110) secondary prism in ice grown in the presence of sculpin AFP is reported [81]. The sculpin AFP is responsible for the growth of prismatic (2  $\bar{1}$  0) ice crystals, where (2  $\bar{1}$  0) is symmetrically identical to (110) [5, 85]. Combinations of secondary prisms with primary (and other secondary) forms are not ruled out theoretically. Indeed, ice crystallites grown out of a solution with AFGPs exhibit ( $hk0$ ) surfaces [86], sometimes in combination with the primary surface (100) [87]. It is easier to observe the difference of secondary face orientations in the case of bipyramids. PBC in [010] is the most strongly bonded PBC contained in the secondary pyramidal surfaces ( $h0l$ ). A large variety in secondary pyramidal shapes has been observed in terms of height-to-baseline ratios or apical angles (cf. Fig. 2.20). The experimentally observed variety of secondary pyramidal surfaces activated by the fish-type ice binding surface [84] ranges from (302) to higher than (401). Among others, (201) is the most common secondary pyramid triggered by the wild-type sculpin AFP [83] and by the winter flounder AFP type I [88, 89]. However, no explanation has been given for the specific occurrence of (201) [83]. In line with the theoretical formulation, none of the pyramids produced by the fish-type ice binding surface, matches in shape the primary pyramid (101) illustrated in Fig. 2.20. As predicted, secondary pyramids appear in combination with primary (and other secondary) forms; the bipyramidal crystals depicted in the observations [84] are combined with the basal face (001) and also some unidentified prismatic facets. The theoretically admissible occurrence of combinations of secondary and primary surfaces can be verified in the experimental images. For example, a combination of (201) and (001) is observed [83].

AFPs of the sculpin engage secondary prisms such as (2  $\bar{1}$  0), while AFPs of the winter flounder later engage the secondary pyramid (201) even though both families have closely related and largely hydrophobic ice binding surfaces [83]. The explanation provided in ref. [83] was that although both ice binding surfaces were indeed hydrophobic, they differed in their structure properties, such as the arrangement of their binding intervals. It is reported [83] that the wild type and few sculpin AFP variants produce secondary pyramids with different degrees of activity even though most sculpin AFPs produce prismatic ice crystals. In addition, the origin of the explanation could be due to the ice binding surface structural

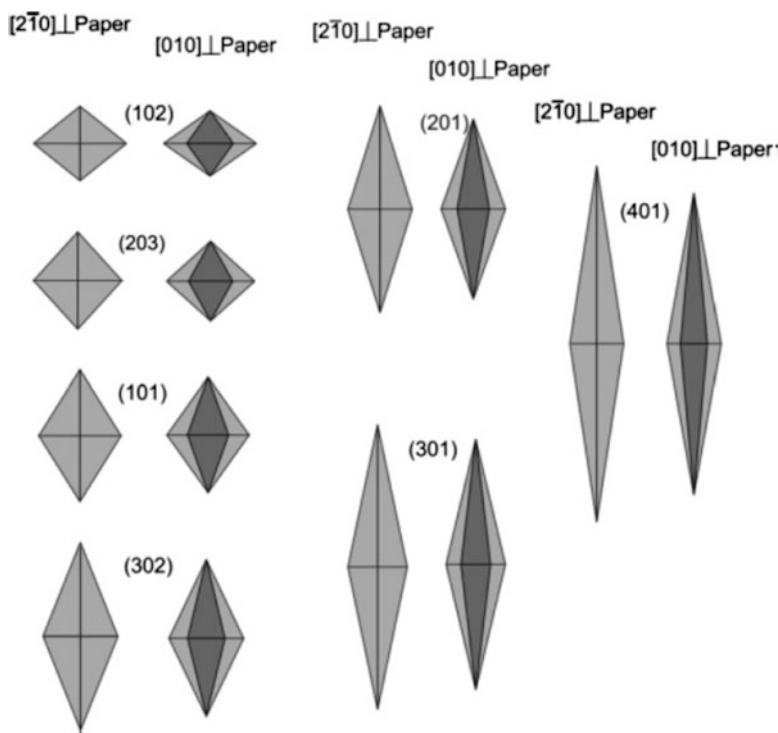


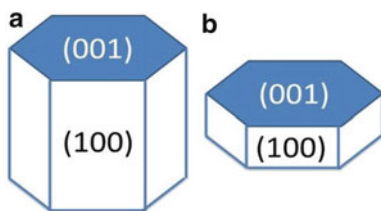
**Fig. 2.20** Outlines of ice pyramidal faces ( $h0l$ ) encountered in a broad range of pyramid-shaped ice crystallites under the influence of (mostly) fish AFPs (absolute size is not to scale). [The ice pyramid face labeled (101) resembles those triggered by the insect TmAFP.] Reprinted with permission from ref. [44]. Copyright (2005) American Chemical Society

aspects. In the work of ref. [90], the addition of divalent ions changes the ice binding surface of the AFP so radically as to transform the crystal shape from secondary to primary facets and vice versa. Moreover, the report on the action of dimer, trimer, and tetramer of type III AFP on ice crystals [91] states that each multimer “changes the morphology of a single ice crystal into a unique shape that is similar but not identical to the ordinary hexagonal bipyramid.” The ice binding surface of type III AFP belongs to the irregular globular ice binding surface type. A significant change in the ice binding surface was noted to cause a radical conversion between pyramidal (Fig. 2.2a of ref. [91]) and prismatic (Fig. 2.2c of ref. [91]) forms, leading to a strong, direct correlation between ice binding surface structure and morphology.

It has long been recognized in the literature [5] that the insect AFP’s capacity to suppress freezing is because of its capacity to grip firmly on the ice lattice via its 2D periodic binding intervals attuned to the ice lattice constants. Take the primary prism (100) (cf. Fig. 2.21) as an example, the spruce budworm AFP producing the hexagonal disk type [92] morphology (Fig. 2.21b) has regular binding intervals in two directions equal to  $\sim 4.5$  and  $7.5$  Å, matching the periods of the strong bonding



**Fig. 2.21** Structural morphology of hexagonal ice



directions  $[010]$  and  $[001]$ . The characteristic morphology of ice grown from most insect AFP solutions is hexagonal plates [5, 92]. In contrast to the structural or the natural morphology, these ice crystallites reveal a strongly pronounced basal face (001) and a morphologically much weakened primary prism (100). In all ice crystallites grown as basal and primary prismatic forms, resulting from layer-by-layer growth, triggered, e.g., by the spruce budworm AFP, no deviation from the  $\{001\}$  and  $\{100\}$  indices has been observed under all experimental conditions. One presumed exception to the hexagonal disk form is found in the action of the TmAFP, the presence of which gives rise to a pyramidal ice habit. It is traditionally held that the action of the insect TmAFP is deviant in causing a pyramidal rather than a disk-shaped morphological modification, whereas all other known insect AFPs cause a hexagonal plate habit. The question arises in the case of the TmAFP as to whether the mechanism of morphological modification is exceptional; that means, whether the ice binding surface of the TmAFP acts on secondary ice surfaces by an exceptional mechanism or on primary ice surfaces by surface pinning through 2D PBC matching, just like the remaining insect-type ice binding surfaces. What this question amounts to is whether the pyramidal ice form observed in the presence of the TmAFP is one of the secondary pyramids with variable indices ( $h0l$ ) or the primary pyramid (101). It is found that the ice bipyramid triggered by the TmAFP [93] has consistently a stubby lemon shape, showing no variation in the apical angle, so that the TmAFP gives rise to a pyramid of fixed indices. The lemon-shaped ice bipyramid produced by the TmAFP is not elongated like the predominant (201) or higher-indexed pyramids observed in connection with the fish AFPs. From the assortment of pyramidal shapes, it can be seen that this bipyramid matches well the primary surface (101). Also in all ice crystallites grown as primary pyramidal forms triggered by the TmAFP, resulting from layer-by-layer growth, no deviation from the  $\{101\}$  indices has been observed under all experimental conditions. Thus, the TmAFP action is by no means exceptional. According to Liou et al. [94], the TmAFP has a high tendency to form hydrogen bonds with an ice surface. This result agrees with the theoretical observation that there are 30% more unbonded hydrogen atoms on the (101) than in the other primary surfaces, pointing to an increased interaction between the ice binding surface of the TmAFP and the (101) primary pyramid [80].

Lastly, it is worth mentioning that although freezing inhibition is always accompanied by a modification of the morphology of the ice crystallites, the converse does not hold true: a morphological modification of ice does not necessarily imply that



the freezing point has been depressed [44]. This is because a change in morphology can have different causes and can be accompanied by total protein inactivity [5, 84, 95]. The particular ice morphology observed is a direct consequence of the structural details related to the adsorption mechanism of the AFP on the ice surfaces, such that different modes of adsorption trigger different crystal habits consistently and predictably.

## 2.4 Applications of AFPs

Any organic compound with the ability to inhibit the growth of ice has many potential medical, industrial, and commercial applications. Although AFPs have potential uses in all of these areas, this review highlights the medical [96, 97] and food [98] applications of AFPs.

### 2.4.1 Cryoprotection

Many complex processes occur when the cell ambient temperature is lowered near to or below that of the freezing point. Physical cell rupture, necrosis, and cold-induced apoptosis are presently the three distinct modes of cell death that occur upon freezing [99]. Although all three processes are significant, the most common form of cell death associated with cryopreservation is cell rupture owing to fluctuating cell volumes and intracellular ice formation [100–104] and, consequently, in this section cell damage will be emphasized because of membrane rupture followed by intracellular ice formation.

Much effort has been dedicated to developing enhanced cryoprotectants and preservation techniques after an accidental discovery that glycerol enabled fowl spermatozoa to survive freezing at  $-70^{\circ}\text{C}$ . All cells are regarded as compartmentalized systems and the probability of ice nucleation is directly proportional to the degree of supercooling and volume. Consequently, as the temperature is lowered, ice nucleation is more likely to occur outside of the cell since the volume is greater and the concentration of colligatively acting substances (salts, proteins, and so forth) is lower than inside the cell. After nucleation occurs, extracellular ice growth results in an increase in solute concentration in the diminishing extracellular volume. As the concentration of these solutes increases, extracellular osmotic pressure increases. The rate at which osmotic pressure increase occurs is directly proportional to the rate of supercooling and this osmotic flux is compensated by the cell through the regulation in the flow of water through the semipermeable cell membrane. Fracturing of the cell membrane is possible when the rate of extracellular ice growth is rapid. Upon the occurrence of the fracture, intracellular ice formation occurs leading to the destruction of the cell. Debates have been going on by researchers as

to whether the ice or elevated salt concentration is the cause for damage during the progressive freezing of cells. The effect of the cooling rate on water transport during progressive cooling was demonstrated by Mazur et al. [105] and they correlated this with cell survival. This eventually leads to a “two factor hypothesis,” which states that solute damage occurs at low cooling rates where extracellular ice formation is innocuous to the cells. On the contrary, at high cooling rates, intracellular ice formation is generally lethal. Cryoprotectant is correlated with an optimum cooling rate since there is a dramatic variation in the membrane permeability of each cell type.

The issues surrounding the cryopreservation of multicellular systems, such as tissues and organs, are infinitely more complex given that many cell types exist and each will differ in the requirements for optimal preservation. The most considerable obstacle to the cryopreservation of multicellular systems is likely to be extracellular ice formation, which leads to the focus on the use of various cryoprotectants that possess the ability to regulate the formation of extracellular ice. Thus, effective cryopreservation of such systems would be expected to occur through an “ice-free” cooling or vitrification process even though this necessitates a high concentration of cryoprotectant. The issue of toxicity arises due to the greatly limited concentration that a tissue can tolerate before freezing. In addition, an osmotic imbalance is inevitable as cryoprotectants penetrate the cell membrane more slowly than water. Thus, cell volume must be regulated carefully during the addition and removal of cryoprotectants.

Vitrification is a common technique employed for the freezing of cells and tissues to avoid cell damage from ice formation. During this process, the solution transforms into a “glass-like” solid enabling the sample to be frozen under “ice-free” conditions. Despite the attractive features of vitrification, it does possess some limitations. For instance, when dealing with larger volumes the heat transfer in cells, tissues, and organs does not permit vitrification without the risk of crystallization. Consequently, a slow freezing process (0.5–100°C/min cooling rate) is often applied for preservation of large volumes. However, in the vitrification process, a very rapid cooling rate (24–130,000°C/min [106]) is applied, resulting in a glassy or vitreous state, which is dependent on the concentration, viscosity, volume, and cooling rate of the process. Although this high cooling rate minimizes cellular damage, recrystallization can still occur during warming. To avoid the risk of recrystallization, rapid and uniform warming can be achieved using microwaves [107–109].

Two problems unique to vitrification are encountered when using the methodologies outlined earlier. First, the necessary cryoprotectant concentration is very high and is sometimes too toxic for the cell. Although the process is feasible with lower concentrations of cryoprotectants, a higher cooling rate must be used to achieve a vitrified state. Second, some fractionation of the glassy state still occurs. The extent to which this occurs is dependent on the volume and the cooling rate and such relationships have been examined in detail [106]. Vitrification works well with small volumes (i.e., <1  $\mu$ L) even though it is not useful for large volumes. However,

each protocol must be optimized and various cryoprotectants must be used. Some of the most promising cryoprotectant solutions incorporate AFGPs. Not only do they inhibit ice formation at any subzero temperature but they also interact with the cell membrane during the thermotropic phase transition state to avoid leakage, thereby addressing two issues at once. (The second effect will be discussed in Sect. 2.4.2.) Numerous factors that influence the success of post-thaw revival include the nature, the temperature, the concentration of the cryoprotectant, the rate of cooling and warming, the storage temperature, and the speed at which the cryoprotectant is added and removed. AFGPs from Antarctic nototheniid fishes were discovered to have special cryoprotective properties that significantly improve morphological integrity upon cooling. Since, the idea of using AFGP additives was then explored in the directional cooling for the preservation of pig oocytes [110]. Vitrified oocytes were observed not be able to survive the cooling/warming cycle. The primary site of damage was to the oolemma. It was subsequently hypothesized that the oolemma was acting as a site for ice nucleation, although the sample was successfully vitrified. A mixture of AFGP 1–8 was added to the sample in an attempt to overcome this problem. This solution resulted in an 82% survival rate of the oocytes as determined by each oocyte reaching the MI or MII stage during incubation. An explanation based on viscosity was proposed by Rubinsky and Eto [111] to explain why AFGP enhanced oocyte viability. They speculated that AFGPs increased solution viscosity and augmented the probability of an “ice-free” state without nucleation. This is a feasible explanation given that the probability for ice nucleation in aqueous solutions is inversely proportional to solution viscosity [112]. The viscosity of solutions containing varying amounts of AFGP was examined in a comprehensive study on AFGP properties and it was reported that as little as 1 mg/mL of AFGP in solutions caused significant increases in solution viscosity with saturation taking place at 20 mg/mL. The viscosity of an aqueous solution of BSA was measured and compared to that of AFGP of comparable weight and reported that solutions of AFGP were slightly more viscous than solutions of BSA. Similar measurements showed that a 20 mg/mL solution of AFGP is 0.005 M, which was equally effective compared to a 1 M solution of dimethyl sulfoxide (DMSO) a commonly used cryoprotectant for vitrification. Subsequently, by using AFGP solutions that are 200 times less concentrated to produce the same effect, the toxic effects of concentrated DMSO solutions maybe eliminated. This observation implies that AFGP might work well as an effective substitute during cryopreservation by vitrification. It is particularly difficult to cryopreserve mammalian oocytes because low temperatures will disrupt the cytoskeleton [113–115] and harden the zona pellucida [116], causing difficulties for sperm to penetrate and fertilize the oocyte. Limited success has been achieved using murine oocytes with both fast and slow cooling protocols. Although vitrication has been achieved with several species of embryos, variable results are often obtained and reproducibility is a problem. It has been speculated that this variability is a result of devitrification of the sample. DeVries and coworkers [115] studied the vitrification of mouse oocytes using a mixture of 6 M DMSO containing 0.1- and 1-mg/mL solution of AFGP [115]. It was demonstrated by them that cryopreservation using 6 M DMSO supplemented with 1 mg/mL of AFGP resulted in low variation and high survival rates.

### 2.4.2 *Lipid Membrane Stabilization*

It was [117, 118] observed by Rubinsky and coworkers that the external cell membrane integrity was enhanced during cooling, and protection against rupture by AFGP and AFP occurred [119]. They suggested that the enhancement of the membrane integrity was due to the blocking of ion fluxes across the membrane by AFGP. Biological antifreezes were then inferred to be directly interacting with membrane-bound ion channels. However, the suggestion has met with some disagreement [119–121]. It was confirmed a few years later by Hayes et al. [122] that AFGP/AFP enhanced membrane integrity during cooling, but they suggest an alternate mechanism consistent with a nonspecific interaction with the liposome membrane. In this work, four different types of phospholipids which were all phosphatidylcholine derived that contained carboxyfluorescein (CF) probes were used to prepare liposomes. Liposomes were observed to leak up to 50% of the trapped marker as they were cooled through the thermotropic phase transition in the absence of AFGP. During this transition state (typically between 12 and 41°C), both gel and liquid crystalline states of the lipid membrane coexist [122–124], provoking a mismatch of the hydrocarbon chains and ultimately facilitating leakage of the lipid membrane. In the presence of less than 1 mg/mL of AFGP, no leakage was observed during cooling or warming through the thermotropic phase transition. Other proteins were also shown to inhibit leakage. The study by Hayes et al. was further expanded by Wu and Fletcher [125] and they examined interactions of AFGP, AFP type 1–3, and albumin interactions with liposomes as model cell membranes. Because most cell membranes are more complex than a phosphatidylcholine (PC) liposome, they prepared liposomes derived from dielaidoylphosphatidylethanolamine and dielaidoylphosphatidylglycerol. Complex AFGP was found to be extremely effective at preventing leakage from the liposomes as each was cooled through its respective thermotropic phase transition. These researchers concluded that AFGP may interact with the lipid bilayer in one of two ways. NMR studies have suggested that AFGP adopts a threefold left-handed helical conformation. The carbohydrate moieties line up on one side of the helix while the hydrophobic alanine residues line up on the other [126, 127]. With this given arrangement, the hydrophilic carbohydrate moieties might interact with the polar head groups of the lipid bilayer, while the hydrophobic backbone of AFGP was hypothesized to be partially immersed in the lipid bilayer and that this may be sufficient to prevent disruption of the bilayer.

The only AFP I that has been studied with liposomes is the naturally occurring protein TTTT. A concentration of 5 mg/mL of TTTT was found to be able to completely inhibit the leakage of the fluorophore carboxyfluorescein from the center of the liposomes as the liposomes were chilled through their thermotropic phase transition temperature. In contrast, this protection against leakage was not observed when the same experiments were performed with low-molecular-weight fractions of AFGPs. Independent experiments indicated that significant amounts of TTTT remained associated with the lipid portions of the bilayer even after

rewarming of the bilayers after they had been cooled through their  $T_m$ . These results, which suggest hydrophobic interactions in the stabilization mechanism, are interesting, as hydrophobicity has also been identified as a key property required for thermal hysteresis. Studies using the synthetic derivatives XXXX2KE with different lipid mixtures have been recently reported to clarify the mechanism by which TTTT interacts with membranes [128]. The study showed that the overall charge and mutations in XXXX ( $X = T, A, V, I$ ) had a profound effect on the ability of the peptide to stabilize membranes. While TTTT stabilized the model membranes to leakage, all four peptides XXXX2KE destabilized the membranes to leakage. TTTT2KE and AAAA2KE interacted preferentially with the DGDG in the lipid mixture, while VVVV2KE showed no preference for either lipid. The results are consistent with interactions involving the hydrophobic face of AFP I and the model bilayers, which is the same face of the protein that is responsible for antifreeze properties. The different effects correlate with the helicity of the peptides, suggesting that the solution conformation of the peptides has a significant role in determining the effects of the peptides on thermotropic phase transitions of the membrane.

AFGPs was proposed by Tomczak and Crowe [129] to form a monolayer coverage of the surface of the membrane to prevent leakage from phospholipid membranes, blocking transient leakage across the membrane as it is cooled through its thermal phase transition ( $T_m$ ). In contrast, direct interactions between the  $\alpha$ -helical AFP I, TTTT, and liposomes containing plant lipid bilayers (that alter the order of the alkyl chains in the hydrophobic core) were proposed as a mechanism for stabilization, via partial insertion of the N-terminal residues of the peptide into the membrane during chilling.

The proposed role of the hydrophobic residues in the four synthetic analogues (XXXX2KE  $X = T, A, I, V$ ) in interactions with lipids [130] is consistent with the ice growth inhibition properties of these compounds. This ice growth inhibition is directly correlated to the hydrophobic face of the helix being oriented toward the ice at the ice/water interface [131]. However, the results with XXXX2KE [86] and liposomes are also informative in terms of the design of synthetic helical AFPs. While TTTT2KE and VVVV2KE retain antifreeze properties (i.e., thermal hysteresis and modification of ice crystal growth) comparable to the native winter flounder AFP TTTT, the introduction of the additional salt bridges in XXXX2KE leads to a destabilization of membranes, clearly an undesirable property when the goal is enhancement of stabilization of membranes to leakage. Further experiments are required to establish whether the destabilization is due to the large size of the additional 2KE side chains, or the increased hydrophilicity of one face of the helix.

### 2.4.3 Food Technology

Ice crystal morphology plays an important role in the textural and physical properties of frozen and frozen-thawed foods and in processes such as freeze

drying, freeze concentration, and freeze texturization [98]. Size and location of ice crystals are major factors in the quality of thawed tissue products. Smaller ice crystals are preferred in ice cream since large crystals will result in an icy texture. In freeze drying, ice morphology influences the rate of sublimation and several morphological characteristics of the freeze-dried matrix as well as the biological activity of components (e.g., in pharmaceuticals).

Nucleation is the most critical step to control the crystal size distribution during crystallization [132]. The freezing (cooling) rate is usually the parameter used for controlling the size and size distribution of ice crystals in frozen and partly frozen systems. Recently, the use of nucleation agents, AFPs, ultrasound, and pressure freezing methods, known by the generic name of “freezing assisting techniques,” have been proposed to control nucleation and ice morphology [133].

Several potential applications for AFPs have been envisaged in foods [98]. In ice cream manufacture, AFPs have been used to fabricate smaller ice crystals compared to a control [134]. In meat products, ice crystal size is reduced by soaking bovine and ovine muscle in a aqueous solution up to 1 mg/mL of AFP prior to freezing at  $-20^{\circ}\text{C}$  [135]. Preslaughter administration of AFP intravenous injection to lambs reduced ice crystal size and drip loss after thawing [136]. The gel-forming functionality of surimi in both chilled and frozen conditions is also preserved by AFPs. In contrast to conventional cryoprotectants such as sucrose–sorbitol mixtures, AFPs remarkably preserved  $\text{Ca}^{2+}$  ATPase activity of actomyosin during storage and provided better protection [137].

Fungal hydrophobin AFPs repressed ice crystal growth during frozen storage, i.e., ice recrystallization, and modified ice crystal shape in aerated and nonaerated frozen food products as suggested by Unilever patent [138]. Although commercial AFPs are currently available, they are mainly for research or special uses because of their high price. Chemical synthesis and genetic engineering may be a solution to produce cost-effective AFPs, hence the need to promote their applications in frozen food products [139].

## 2.5 AFPs Synthesis and Mimics

### 2.5.1 Antifreeze Glycoproteins Synthesis and Mimics

The synthesis of AFGPs as pure glycoforms has been achieved through using ligation and polymerization strategies, and key structure–activity studies that are essential to inform the design of functional mimics have been reported [140–142].

The AFGPs isolated from fish blood plasma range in molecular mass from approximately 33 kDa (50 repeating units) to 2.6 kDa (four repeating units). They consist of repeating tripeptide units  $(\text{Ala-Thr-Ala})_n$  with a disaccharide moiety (Galb1-3GalNAc1-) attached to each threonyl residue [25]. Nishimura and colleagues reported the first synthesis of AFGPs in the form of pure glycoforms in

2004 [140], in a landmark paper that also reported the first structure–activity studies on AFGPs, and thus provided data that are essential to understanding the mechanism of action and to guiding the design of AFGP mimics. It was reported in an earlier communication polymeric AFGP of molecular weight ( $M_w$ ) = 6–7 k could be efficiently synthesized by simple polymerization of the repeating glycopeptides unit of AFGP with diphenylphosphoryl azide (DPPA) as a promoter [141]. In the presence of the unprotected hydroxyl groups in the sugars, DPPA selectively activates the peptide carboxylic acid and by using this method, glycopeptides polymers of different ranges of molecular weight were produced. Through optimization of the chemistry, polymerization occurs most efficiently when using the glycoside of Ala-Thr-Ala; steric effects are minimized in the polymerization reaction compared with Ala-Ala-Thr with a glycoside C terminus [143]. Additional sugars were also appended enzymatically to the disaccharides [143].

The details of the overall synthesis is described in reference [140]. Low-molecular-weight fractions containing between two and eight repeating units (syAFGP2–syAFGP8) were obtained using a lower temperature and shorter reaction times. Consistent fractions of precise chain lengths containing up to seven repeating units were achieved by using recycling preparative size-exclusion chromatography. The effectiveness of 1-isobutoxycarbonyl-2-isobutoxy-1,2-dihydroquinoline (IIDQ) and 4-(4,6-dimethoxy-1,3,5-triazin-2-yl)-4 methylmorpholinium chloride (DMTMM) versus DPPA was also assessed as promoters for the formation of the glycopolymers [33]. DMT-MM-mediated condensation reactions proceeded smoothly, even though the average molecular weights of the polymers obtained with IIDQ were lower than those obtained with DPPA, and therefore provides a more general reagent for the synthesis of AFGP analogues consisting base-labile functional groups.

The recent NMR solution structure of syAFGP3 showed a significant population of a folded conformation with hydrophilic and hydrophobic faces [140]. This solution structure, and clear evidence for the important role of hydrophobic interactions in the interactions of several classes of AFPs with ice [44, 131, 144, 145] has refocused attention on understanding the possible role of hydrophobicity in the mechanism of action of AFGPs. Of particular note is the high prevalence of Ala and Thr residues in both type I AFPs [145] and AFGPs. It should be noted that AFGP8 at high concentrations (20–40 mM) exists predominately as dimer aggregates with higher thermal hysteresis activity as shown through dynamic light scattering and CD studies [44]. Overall solution conformation does not appear to be affected by these aggregates, and diffusion NMR studies of AFGP8 revealed no evidence for aggregation in solution at biologically relevant conditions [97]. In light of these structural studies, recent solution studies by a variety of techniques have looked for any proof for a preferred conformation of AFGPs at close to 0°C, or a rise in population of folded conformers that might be important in the interaction with the ice/water interfaces. The dynamics, structure, and conformational free energy of AFGP8, the smallest 14-residue AFGP containing two Pro residues, were studied by molecular dynamics [146]. The results confirmed that N-acetyl group plays an important role, with hydrogen bonding between the N-acetyl group and



the peptide backbone detected approximately 43% of the time. It was concluded from the study that AFGP8 has numerous structurally distinct degenerate minima, and this set of low-energy minima was proposed to be important for antifreeze activity. In particular, interconversion among multiple minima of AFGP8 can act as a thermal reservoir that will retard the growth rate of the ice crystal locally where it accumulates on the ice surface. This study overall suggests that conformational flexibility to access a variety of low-energy minima states is critical for antifreeze activity even though the Pro residues have an important role in stabilizing the conformations adopted by the AFGP.

The self-diffusion of AFGP8 as a function of temperature was monitored by NMR spectroscopy (243–303 K) in an independent study to evaluate if AFGPs undergo any global structural rearrangements in the supercooled regime that could be the cause for their function [65]. These results suggested that AFGP is more hydrated (ca. 30% increase in the bead radius) than other globular proteins, but showed no evidence for any major structural reorganization in order to function. Nishiumra et al. have also detected the presence of hydrated forms of syAFGP3 with water molecules by using cold spray ionization time-of-flight mass spectrometry [140]. The involvement of the Thr residue in the hydration of AFGPs is supported by recent studies that have demonstrated that the Thr *g*-methyl group is an important determinant of both the carbohydrate orientation and the degree of hydration [147]. Substituting d-GalNAcThr with d-GalNAcSer affects the strength of hydrogen bond involving the N-acetyl group and results in a significant increase in conformational degrees of freedom as well as the orientation of the neighboring water molecules. Consequently, the evolution of AFGPs with Thr in their structure, rather than Ser, may be attributed to the contribution of Thr to hydrophobicity and hydration effects, as well as the restricted conformational space of Thr glycosides compared with Ser glycosides [142].

The helical content of AFGP in the liquid, supercooled and frozen states of the solution film have been compared by attenuated total reflection (ATR)-FTIR spectroscopy [148]. The results showed that the AFGP molecules do not show any large conformational changes during supercooling whereas they change their conformation and become significantly helical upon freezing. It was proposed that the increase in helicity was to allow the AFGPs to increase the number of adsorption sites and maximize the interaction with ice crystals.

A number of studies on the interaction of AFGPs with surfaces have been carried out to probe the contributions of hydrophobic and hydrophilic interactions to adsorption. These studies are not of direct relevance to the biological mechanism of action of AFGPs, as these surfaces are models for an ice/vacuum interaction. However, such models can provide insights into surface properties such as nucleation events and surface roughening, and have been useful in the delineation of the features required for the assembly and development of functional materials. Sarno et al. examined the adsorption of AFGP8 onto mica and highly ordered pyrolytic graphite (HOPG), which contains both hydrophilic and hydrophobic binding sites (step edges or planes) [149]. The results showed that AFGP8 binds preferentially to the hydrophilic step edges of the surface. It was further shown that AFGP8 deposited



on mica by the solution droplet evaporation technique resulted in patterned surfaces formed by a single layer of protein [150] and that AFGP aggregates prior to deposition. Raman spectroscopy has also been used to monitor the interaction of AFGP8 on HOPG and Ag-coated glass-ceramic surfaces [151, 152].

A novel attempt to mimic the active domain of AFGPs in a simple monolayer is achieved by Hederos et al. A disaccharide-functionalized alkyl thiol chain was co-adsorbed with C<sub>2</sub>H<sub>5</sub>OC<sub>2</sub>H<sub>4</sub>NHCOC<sub>15</sub>H<sub>30</sub>SH to form statistically mixing self-assembled monolayers on gold [153]. Ice crystallization was examined by optical microscopy as the surface was cooled under an atmosphere of constant relative humidity. Water molecules appeared to organize and nucleate onto the self-assembled monolayer surface with high disaccharide content (>30%, i.e., the same ratio as AFGP) with behavior consistent with the absorption–inhibition model of AFGPs. Nonetheless, any direct comparison between the results with this system and native AFGPs is not yet possible as noted by the authors.

### 2.5.2 Protein-Based Anti-Ice Coating

The described features of AFPs are very interesting for nano(bio)technological applications, and the feasibility of both anti-ice and ice nucleation coatings has been demonstrated in proof-of-concept studies [154]. Wierzbicki et al. [155] described the structure–function relationship of a de novo synthesized 43-residue alanine–lysine-rich antifreeze polypeptide that is able to bind to designated ice planes along a specific direction [155]. A new protein-based ice-nucleating coating containing locally isolated nucleation points in a low surface energy matrix was synthesized by Zwieg et al. [156] using a sol–gel method. In addition to ice nucleation, this coating also displayed improved ice-repellent properties compared with commercial coatings. In addition, inspired by the sacred lotus leaf, anti-icing of surfaces has been performed with superhydrophobic coatings [157].

A feasibility study to modify lacquer surfaces with AFPs was conducted at the Fraunhofer IFAM, Germany [158]. Winter flounder and the European fir budworm were chosen as suitable AFP model organisms. Defined peptide sequences were produced by solid-phase peptide synthesis on a laboratory scale. Three different strategies were used to achieve the bonding of the artificial AFP residues to commercially available lacquer systems. The first approach consists of spraying an aqueous protein solution onto the lacquer by means of an ultrasound nebulizer. The coating system contained epoxy resin and a polyamine hardener. The epoxide groups on the lacquer surface reacted with the amino groups of the proteins and the protein became incorporated into the polymer. The second approach involves integrating photochemically active molecule into the lacquer system and AFPs were attached by photochemical means. The third approach consists of attaching the peptides to the lacquer via linker molecules, thus displaying the AFP residues on the surface. Among the three approaches, the third approach proved to be very promising. Control tests were carried out with various coating setups in a frosting chamber

at controlled airflow temperatures. Considerably less ice formed on the AFP-functionalized surfaces in contrast to the control, while a nonuniform coating also resulted in nonuniform frosting patterns. The results demonstrate both the feasibility and the enormous potential of biomimetic antifreeze coatings based on AFPs.

## 2.6 Conclusions and Outlook

The strategies employed by diverse organisms to cope with the cold provide fascinating insights into the adaptability of life on Earth. Continuing research into the molecular mechanisms of cold adaptation and freezing survival offer valuable insights into the molecular mechanisms of structure–function relationships, such as the case of what people have found about AFPs. Furthermore, these studies provide unique opportunities to identify new key applications for biotechnology advancement, such as improved freeze tolerance in plants and cold hardiness in animals, organ cryopreservation, and the destruction of malignant tumors in cryosurgery in medicine.

## References

1. Mutaftschiev, B.: In: Hurle, D.T.J. (ed.) *Handbook of Crystal Growth*. North-Holland, Amsterdam, The Netherlands (1993)
2. Davies, P.L., Sykes, B.D.: Antifreeze proteins. *Curr. Opin. Struct. Biol.* **7**, 828–834 (1997)
3. Davies, P.L., Hew, C.L.: Biochemistry of fish antifreeze proteins. *FASEB J.* **4**, 2460–2468 (1990)
4. Knight, C.A.: Adding to the antifreeze agenda. *Nature* **406**, 249–251 (2000)
5. Jia, Z.C., Davies, P.L.: Antifreeze proteins: an unusual receptor–ligand interaction. *Trends Biochem. Sci.* **27**, 101–106 (2002)
6. Liu, X.Y.: Simulating ‘atomic’ processes of crystallization via controlled colloidal assembly. In: Wang, M., Tsukamoto, K., Wu, D. (eds.) *Selected Topics on Crystal Growth: 14th International Summer School on Crystal Growth*, pp. 173–220. American Institute of Physics, Dalian (2010)
7. Liu, X.Y.: From templated nucleation to functional materials engineering. In: Skowronski, M., DeYoreo, J.J., Wang, C.A. (eds.) *Perspectives on Inorganic, Organic and Biological Crystal Growth: from Fundamentals to Applications*, pp. 439–465. American Institute of Physics, Park City, UT (2007)
8. Liu, X.Y.: From molecular structure of solid–fluid interfaces to nucleation kinetics: implications for nanostructure engineering. In: De Yoreo, J., Liu, X.Y. (eds.) *Nanoscale Structure and Assembly at Solid–Fluid Interfaces*. **1**, Springer (2004)
9. Liu, X.Y.: Generic mechanism of heterogeneous nucleation and molecular interfacial effects. In: Sato, K., Nakajima, K., Furukawa, Y. (eds.) *Advances in Crystal Growth Research*, pp. 42–61. Elsevier Science B.V., Amsterdam (2001)
10. Koop, T., et al.: A new optical technique to study aerosol phase transitions: the nucleation of ice from H<sub>2</sub>SO<sub>4</sub> aerosols. *J. Phys. Chem. A* **102**(45), 8924–8931 (1998)
11. Hare, D.E., Sorensen, C.M.: The density of supercooled water. II. Bulk samples cooled to the homogeneous nucleation limit. *J. Chem. Phys.* **87**(8), 4840–4845 (1987)

12. Liu, X.Y., Du, N.: Zero-sized effect of nano-particles and inverse homogeneous nucleation: principles of freezing and antifreeze. *J. Biol. Chem.* **279**, 6124–6131 (2004)
13. Liu, X.Y., et al.: Prediction of crystal growth morphology based on structural analysis of the solid–fluid interface. *Nature* **374**(6520), 342–345 (1995)
14. Liu, X.-Y., Bennema, P.: Morphology of crystals: internal and external controlling factors. *Phys. Rev. B* **49**(2), 765–775 (1994)
15. Liu, X.Y., et al.: Analysis of morphology of crystals based on identification of interfacial structure. *J. Chem. Phys.* **103**(9), 3747–3754 (1995)
16. Liu, X.-Y., Bennema, P.: Theoretical consideration of the growth morphology of crystals. *Phys. Rev. B* **53**(5), 2314–2325 (1996)
17. Liu, X.Y.: Modeling of the fluid-phase interfacial effect on the growth morphology of crystals. *Phys. Rev. B* **60**(4), 2810–2817 (1999)
18. DeVries, A.L.: *Survival at freezing temperatures*. In: Sargent, J.M., Malins, D.C. (eds.) *Biochemical and Biophysical Perspectives in Marine Biology*, pp. 289–330. Academic Press, London (1974)
19. Duman, J.G., Olsen, T.M.: Thermal hysteresis protein activity in bacteria, fungi, and phylogenetically diverse plants. *Cryobiology* **30**, 322–328 (1993)
20. Yeh, Y., Feeney, R.E.: Antifreeze proteins-structures and mechanisms of function. *Chem. Rev.* **96**, 601–617 (1996)
21. Graham, L.A., Liou, Y.-C., Walker, V.K., Davies, P.L.: Hyperactive antifreeze protein from beetles. *Nature* **388**, 727–728 (1997)
22. Scholander, P.F., Dam, L.V., Kanwisher, J., Hammel, T., Gordon, M.S.: Supercooling and osmoregulation in Arctic fish. *J. Cell. Comp. Physiol.* **49**, 5–24 (1957)
23. Gordon, M.S., Amdur, B.H., Scholander, P.F.: Freezing resistance in some northern fishes. *Biol. Bull.* **122**, 52–62 (1962)
24. DeVries, A.L.: Freezing resistance in some Antarctic fishes. *Science* **163**, 1073–1075 (1969)
25. DeVries, A.L., Komatsu, S.K., Feeney, R.E.: Chemical and physical properties of freezing point-depressing glycoproteins from Antarctic fishes. *J. Biol. Chem.* **245**, 2901–2908 (1970)
26. Duman, J.G., DeVries, A.L.: Freezing behaviour of aqueous solutions of glycoproteins from the blood of an Antarctic fish. *Cryobiology* **9**, 469–472 (1972)
27. Lin, Y., Duman, J.G., DeVries, A.L.: Studies on the structure and activity of lowmolecular weight glycoproteins from an Antarctic fish. *Biochem. Biophys. Res. Commun.* **46**, 87–92 (1972)
28. Raymond, J.A., DeVries, A.L.: Freezing behaviour of fish blood glycoproteins with antifreeze properties. *Cryobiology* **9**, 541–547 (1972)
29. Scholander, P.F., Maggert, J.E.: Supercooling and ice propagation in blood from Arctic fishes. *Cryobiology* **8**, 371–374 (1971)
30. Fletcher, G.L., Hew, C.L., Davies, P.L.: Antifreeze proteins of Teleost fishes. *Annu. Rev. Physiol.* **63**, 359–390 (2001)
31. Jia, Z., Davies, P.L.: Antifreeze proteins: an unusual receptor–ligand interaction. *Trends Biochem. Sci.* **2**, 101–106 (2002)
32. Duman, J.G., DeVries, A.L.: Freezing resistance in winter flounder *Pseudopleuronectes americanus*. *Nature* **247**, 237–238 (1974)
33. Ng, N.F., Trinh, K.-Y., Hew, C.L.: Structure of an antifreeze polypeptide precursor from the sea raven, *Hemirhamphus americanus*. *J. Biol. Chem.* **261**, 15690–15695 (1986)
34. Jia, Z.C., Deluca, C.I., Davies, P.L.: Crystallization and preliminary X-ray crystallographic studies on type III antifreeze protein. *Protein Sci.* **4**, 1236–1238 (1995)
35. Deng, G.J., Andrews, D.W., Laursen, R.A.: Amino acid sequence of a new type of antifreeze protein—from the longhorn sculpin *Myoxocephalus octodecimspinosus*. *FEBS Lett.* **402**, 17–20 (1997)
36. DeVries, A.L.: Glycoproteins as biological antifreeze agents in Antarctic fishes. *Science* **172**, 1152–1155 (1971)
37. Ramsay, R.A.: The rectal complex of the mealworm (*Tenebrio molitor* L. *Coleoptera*, *Tenebrionidae*). *Philos. Trans. R. Soc. London Ser. B* **248**, 279–314 (1964)

38. Duman, J.G.: Subzero temperature tolerance in spiders: the role of thermal hysteresis factors. *J. Comp. Physiol.* **131**, 347–352 (1979)
39. Block, W., Duman, J.G.: Presence of thermal hysteresis producing antifreeze proteins in the Antarctic mite *Alaskozetes antarcticus*. *J. Exp. Zool.* **250**, 229–231 (1989)
40. Tursman, D., Duman, J.G., Knight, C.A.: Freeze tolerance adaptations in the centipede *Lithobius forficatus*. *J. Exp. Zool.* **268**, 347–353 (1994)
41. Duman, J.G.: Antifreeze and ice nucleator proteins in terrestrial arthropods. *Annu. Rev. Physiol.* **63**, 327–357 (2001)
42. Urrutia, M.E., Duman, J.G., Knight, C.A.: Plant thermal hysteresis proteins. *Biochim. Biophys. Acta* **1121**, 199–206 (1992)
43. Pauling, L.: The structure and entropy of ice and of other crystals with some randomness of atomic arrangement. *J. Am. Chem. Soc.* **57**, 2680–2684 (1935)
44. Strom, C.S., Liu, X.Y., Jia, Z.: Ice surface reconstruction as antifreeze protein-induced morphological modification mechanism. *J. Am. Chem. Soc.* **127**, 428–440 (2005)
45. Zhang, K.-Q., Liu, X.Y.: In situ observation of colloidal monolayer nucleation driven by an alternating electric field. *Nature* **429**(6993), 739–743 (2004)
46. Liu, X.Y.: From molecular structure of solid-fluid interfaces to nucleation kinetics: implications for nanostructure engineering. In *Nanoscale structure and assembly at solid-fluid interfaces*, edited by X.Y. Liu, and James J. De Yoreo, Springer, London, Vol.I, p. 109–175 (2004)
47. Fowler, R., Guggenheim, E.A.: *Statistical Thermodynamics*. Cambridge University, London (1960)
48. Diao, Y.Y., Liu, X.Y.: Controlled colloidal assembly: experimental modeling of general crystallization and biomimicking of structural color. *Adv. Funct. Mater.* **22**(7), 1354–1375 (2012)
49. Liu, X.Y.: Generic mechanism of heterogeneous nucleation and molecular interfacial effects. In *Advances in Crystal Growth Research*, edited by K.Sato, K.Nakajima and Y. Furukawa ELSEVIER SCIENCE B.V., Amsterdam, 42–61 (2001)
50. Liu, X.Y.: A new kinetic model for 3D heterogeneous nucleation, compared with experiments. *J. Chem. Phys.* **111**, 1628–1635 (1999)
51. Du, N., Liu, X.Y.: Controlled ice nucleation in micro-sized water droplet. *Appl. Phys. Lett.* **81**, 445–447 (2002)
52. Rasmussen, D.H.: Thermodynamics and nucleation phenomena—a set of experimental observations. *J. Cryst. Growth* **56**, 56–66 (1982)
53. Mullin, J.W.: *Crystallization*, pp. 182–194. Butterworth-Heinemann, Oxford (1997)
54. Du, N., Liu, X.Y.: Ice nucleation inhibition: mechanism of antifreeze by antifreeze protein. *J. Biol. Chem.* **278**, 36000–36004 (2003)
55. Liu, X.-Y., Bennema, P., van der Eerden, J.P.: Rough-flat-rough transition of crystal surfaces. *Nature* **356**(6372), 778–780 (1992)
56. Liu, X.-Y., van Hoof, P., Bennema, P.: Surface roughening of normal alkane crystals: solvent dependent critical behavior. *Phys. Rev. Lett.* **71**(1), 109–112 (1993)
57. Liu, X.-Y., Bennema, P.: The equilibrium state of solid-liquid interfaces of aliphatic compounds. *J. Chem. Phys.* **97**(5), 3600–3609 (1992)
58. Liu, X.-Y.: First-order thermal roughening of normal alkane crystals. *Phys. Rev. B* **48**(3), 1825–1829 (1993)
59. Liu, X.-Y., Bennema, P.: Self-consistent-field calculation of structures and static properties of the solid-fluid interface: paraffinlike molecule systems. *Phys. Rev. E* **48**(3), 2006–2015 (1993)
60. Liu, X.-Y., Bennema, P.: The relation between macroscopic quantities and the solid-fluid interfacial structure. *J. Chem. Phys.* **98**(7), 5863–5872 (1993)
61. Xiang-Yang, L.: The solid-fluid interface: a comparison and further description using the layer model. *Surf. Sci.* **290**(3), 403–412 (1993)
62. Liu, X.-Y.: Properties and structure of crystal-solution interfaces of normal alkane crystals: influence of solvents. *J. Chem. Phys.* **102**(3), 1373–1384 (1995)

63. Liu, X.Y., et al.: Can a foreign particle cause surface instability? *J. Phys. Chem. B* **104**(50), 11942–11949 (2000)
64. Liu, X.Y.: Effect of foreign particles on the growth of faceted crystal faces. *J. Chem. Phys.* **113**(19), 8807–8816 (2000)
65. Liu, X.Y., Bennema, P.: Foreign body induced kinetic roughening: kinetics and observations. *J. Chem. Phys.* **115**(9), 4268–4274 (2001)
66. Zhang, K.-Q., Liu, X.Y.: Two scenarios for colloidal phase transitions. *Phys. Rev. Lett.* **96**(10), 105701 (2006)
67. Liu, X.Y., Maiwa, K., Tsukamoto, K.: Heterogeneous two-dimensional nucleation and growth kinetics. *J. Chem. Phys.* **106**(5), 1870–1879 (1997)
68. Chernov, A.A.: *Modern Crystallography III Crystal Growth*. Springer Verlag, Berlin (1984)
69. Liu, X.Y.: Interfacial effect of molecules on nucleation kinetics. *J. Phys. Chem. B* **105**(47), 11550–11558 (2001)
70. Strom, C. S.: Graph-theoretic construction of Periodic Bond Chains I, General Case. *Z. Kristallogr.* **153**, 99–113 (1980)
71. Hartman, P.: The dependence of crystal morphology on crystal structure. In: Sheftal, N.N. (ed.) *Growth of Crystals*, pp. 3–18. Consultants Bureau, New York (1969)
72. Strom, C.S.: Ionic crystals. In: Myerson, A.S. (ed.) *Molecular Modeling Applications in Crystallization*, pp. 228–312. Cambridge University Press, New York (1999)
73. Donnay, J.D.H.: *Spherical Trigonometry after the Cesàro Method*. Interscience Publishers, Inc., New York, NY (1945)
74. Hartman, P., Perdok, W.G.: On the relations between structure and morphology of crystals. II. *Acta Crystallogr.* **8**(9), 521–524 (1955)
75. Hartman, P., Perdok, W.G.: On the relations between structure and morphology of crystals. III. *Acta Crystallogr.* **8**(9), 525–529 (1955)
76. Hartman, P., Perdok, W.G.: On the relations between structure and morphology of crystals. I. *Acta Crystallogr.* **8**(1), 49–52 (1955)
77. Hartman, P., Bennema, P.: The attachment energy as a habit controlling factor: I. Theoretical considerations. *J. Cryst. Growth* **49**(1), 145–156 (1980)
78. Bennema, P.: Thermodynamics and kinetics. In: Hurle, D.T.J. (ed.) *Handbook of Crystal Growth 1a Fundamentals*, pp. 477–581. Elsevier, Amsterdam (1993)
79. Strom, C.S., Liu, X.Y., Jia, Z.: Antifreeze protein-induced morphological modification mechanisms linked to ice binding surface. *J. Biol. Chem.* **279**, 32407–32417 (2004)
80. Strom, C.S., Liu, X.Y., Jia, Z.: Why does insect antifreeze protein from *Tenebrio molitor* produce pyramidal ice crystallites? *Biophys. J.* **89**, 2618–2627 (2005)
81. Baardsnes J., Jelokhani-Niaraki, M., Kondejewski, L.H., Kuiper, M.J., Kay, C.M., Hodges, R.S., Davies, P.L. Antifreeze protein from shorthorn sculpin: identification of the ice-binding surface. *Protein Sci.* **10**, 2566–2576 (2001)
82. Zhang, W.L.: Artificial antifreeze polypeptides:  $\alpha$ -helical peptides with KAAK motifs have antifreeze and ice crystal morphology modifying properties. *FEBS Lett.* **455**, 372–376 (1999)
83. Fairley, K., Westman, B.J., Pham, L.H., Haymet, A.D. J., Harding, M.M., Mackay, J.P. Type I shorthorn sculpin antifreeze protein - Recombinant synthesis, solution conformation, and ice growth inhibition studies. *J. Biol. Chem.* **277**, 24073–24080 (2002).
84. Houston, M.E., Chao, H., Hodges, R.S., Sykes, B.D., Kay, C.M., Sonnichsen, F.D., Loewen, M.C., Davies, P.L.: Binding of an oligopeptide to a specific plane of ice. *J. Biol. Chem.* **273**, 11714–11718 (1998)
85. Wierzbicki, A., Taylor, M.S., Knight, C.A., Madura, J.D., Harrington, J.P., Sikes, C.S.: Analysis of shorthorn sculpin antifreeze protein stereospecific binding to (2–10) faces of ice. *Biophys. J.* **71**, 8–18 (1996)
86. Harding, M.M., Anderberg, P.I., Haymet, A.D.J.: ‘Antifreeze’ glycoproteins from polar fish. *Eur. J. Biochem.* **270**(7), 1381–1392 (2003)
87. Wilson, P.W., Gould, M., Devries, A.L. Hexagonal shaped ice spicules in frozen antifreeze protein solutions. *Cryobiology* **44**, 240–250 (2002)

88. Harding, M.M., Ward, L.G., Haymet, A.D. Type I 'antifreeze' proteins. Structure-activity studies and mechanisms of ice growth inhibition. *Eur J Biochem*, **264**, 653–665 (1999).
89. Haymet, A.D., Ward, L.G., Harding, M.M., Knight, C.A.: Valine substituted winter flounder 'antifreeze': preservation of ice growth hysteresis. *FEBS Lett.* **430**, 301–306 (1998)
90. Ewart, K.V., Yang, D.S.C., Ananthanarayanan, V.S., Fletcher, G.L., Hew, C.L.: Ca<sup>2+</sup>-dependent antifreeze proteins modulation of conformation and activity by divalent ions. *J. Biol. Chem.* **271**, 16627–16632 (1996)
91. Nishimiya, Y., Ohgiya, S., Tsuda, S.: Artificial Multimers of The Type III Antifreeze Protein: Effects on Thermal Hysteresis and Ice Crystal Morphology. *J. Biol. Chem.*, **278**, 32307–32312 (2003).
92. Graether, S.P., Kuiper, M.J., Gagn, S.M., Walker, V.K., Jia, Z., Sykes, B.D., Davies, P.L.:  $\beta$ -Helix structure and ice-binding properties of a hyperactive antifreeze protein from an insect. *Nature* **406**, 325–328 (2000)
93. Wathen, B., Kuiper, M., Walker, V., Jia, Z. A new model for simulating 3D crystal growth and its application to the study of antifreeze proteins. *J. Am. Chem. Soc.* **125**, 729–737 (2003).
94. Liou, Y.-C., Tocilj, A., Davies, P.L., Jia, Z.: Mimicry of ice structure by surface hydroxyls and water of a  $\beta$ -helix antifreeze protein. *Nature* **406**, 322–324 (2000)
95. Baardsnes, J., Kondejewski, L.H., Hodges, R.S., Chao, H., Kay, C., Davies, P.L.: New ice-binding face for type I antifreeze protein. *FEBS Lett.* **463**, 87–91 (1999)
96. Bouvet, V., Ben, R.N.: Antifreeze glycoproteins structure, conformation, and biological applications. *Cell Biochem. Biophys.* **39**, 133–144 (2003)
97. Inglis, S.R., Turner, J.J., Harding, M.M.: Applications of type I antifreeze proteins: studies with model membranes & cryoprotectant properties. *Curr. Protein Pept. Sci.* **7**, 509–522 (2006)
98. Aguilera, G.P.J.M.: Ice morphology: fundamentals and technological applications in foods. *Food Biophys.* **4**, 378–396 (2009)
99. Baust, J.M.: Molecular mechanisms of cellular demise associated with cryopreservation failure. *Cell Preserv. Technol.* **1**, 17–31 (2002)
100. Glander, A.J., Schaller, J.: Binding of annexin V to plasma membranes of human spermatozoa: a rapid assay for detection of membrane changes after cryostorage. *Mol. Hum. Reprod.* **5**, 109–115 (1999)
101. Baust, J.M., Van Buskirk, R.G., Baust, J.G.: Cell viability improves following inhibition of cryopreservation-induced apoptosis. *In Vitro Cell. Dev. Biol. Anim.* **36**, 262–270 (2000)
102. Fowke, K.R., Behnke, J., Hanson, C., Shea, K., Cosentino, M.: Apoptosis: a method for evaluating the cryopreservation of whole blood mononuclear cells. *J. Immunol. Methods* **244**, 139–144 (2000)
103. Hilbert, S.L., Luna, R.E., Zhang, J., Wang, Y., Hopkins, R.A., Yu, Z.X., Ferran, V.T.: Allograft heart valves: the role of apoptosis-mediated cell loss. *J. Thorac. Cardiovasc. Surg.* **117**, 454–462 (1999)
104. Villalba, R., Pena, J., Luque, E., Gomez-Villagran, J.L.: Characterization of ultrastructural damage of valves cryopreserved under standard conditions. *Cryobiology* **43**, 81–84 (2001)
105. Mazur, P.: Kinetic of water loss from cells at subzero temperatures and the likelihood of intracellular freezing. *J. Gen. Physiol.* **47**, 347–369 (1963)
106. Arav, A., Yavin, S., Zeron, Y., Natan, D., Dekel, I., Gacitua, H.: New trends in gamete's cryopreservation. *Mol. Cell. Endocrinol.* **187**, 77–81 (2002)
107. Marsland, T.P., Evans, S., Pegg, D.E.: Dielectric measurements for design of an electromagnetic rewarming system. *Cryobiology* **24**, 311–323 (1981)
108. Robinson, M.P., Pegg, D.E.: Rapid electromagnetic warming of cells and tissues. *IEEE Trans. Biomed. Eng.* **46**, 1413–1425 (1999)
109. Pegg, D.E.: The history and principles of cryopreservation. *Semin. Reprod. Med.* **20**, 5–13 (2002)
110. Rubinsky, B., Arav, A., Devries, A.L.: Cryopreservation of oocytes using directional cooling and antifreeze glycoproteins. *Cryo Lett.* **12**, 93–106 (1991)



111. Eto, T.K., Rubinsky, B.: Antifreeze glycoproteins increase solution viscosity. *Biochem. Biophys. Res. Commun.* **197**, 927–931 (1993)
112. Wu, Y., Banoub, J., Goddard, S.V., Kao, M.H., Fletcher, G.L.: Antifreeze glycoproteins: relationship between molecular weight, thermal hysteresis and the inhibition of leakage from liposomes during thermotropic phase transition. *Comp. Biochem. Physiol. B* **128**, 265–273 (2001)
113. Pickering, S.J., Braude, P.R., Johnson, M.H., Can, A., Currie, J.: Transient cooling to room temperature can cause irreversible disruption of the meiotic spindle in the human oocyte. *Fertil. Steril.* **54**, 102–108 (1990)
114. Pickering, S.J., Johnson, M.H.: The influence of cooling on the organization of the meiotic spindle of the mouse oocyte. *Hum. Reprod.* **2**, 207–216 (1987)
115. O’Neil, L., Paynter, S.J., Fuller, B.J., Shaw, R.W., DeVries, A.L.: Vitrification of mature mouse oocytes in a 6 M Me2SO solution supplemented with antifreeze glycoproteins: The effect of temperature. *Cryobiology* **37**, 59–66 (1998)
116. Vincent, C., Johnson, M.H.: Cooling, cryoprotectants, and the cytoskeleton of the mammalian oocyte. *Oxford Rev. Reprod. Biol.* **14**, 73–100 (1992)
117. Rubinsky, B., Arav, A., Devries, A.L.: The cryoprotective effect of antifreeze glycopeptides from Antarctic fishes. *Cryobiology* **29**, 69–79 (1992)
118. Storey, K.B., Bischof, J., Rubinsky, B.: Cryomicroscopic analysis of freezing in liver of the freeze tolerant wood frog. *Am. J. Physiol.* **263**, R185–R194 (1992)
119. Hinch, D.K., Devries, A.L., Schmitt, J.M.: Cryotoxicity of antifreeze proteins and glycoproteins to spinach thylakoid membranes—comparison with cryotoxic sugar acids. *Biochim. Biophys. Acta* **1146**, 258–264 (1993)
120. Cheng, C., Devries, A.L.: Do antifreeze proteins have a role in maintenance of ion gradients across cell membranes in polar fishes and invertebrates? *Cryobiology* **29**, 783 (1992)
121. Payne, S.R., Oliver, J.E., Upreti, G.C.: Effect of antifreeze proteins on the motility of ram spermatozoa. *Cryobiology* **31**, 180–184 (1994)
122. Hays, L., Feeney, R.E., Crowe, L.M., Crowe, J.H., Oliver, A.E.: Antifreeze glycoproteins inhibit leakage from liposomes during thermotropic phase transitions. *Proc. Natl. Acad. Sci. U.S.A.* **93**, 6835–6840 (1996)
123. Quinn, P.J.: A liquid-phase separation model of low temperature damage to biological membranes. *Cryobiology* **22**, 128–146 (1995)
124. Clerc, S.G., Thompson, T.G.: Permeability of dimyristoyl phosphatidylcholine/dipalmitoyl phosphatidylcholine bilayer-membranes with coexisting gel and liquid-crystalline phases. *Biophys. J.* **68**, 2333–2341 (1995)
125. Wu, Y., Fletcher, G.L.: Efficacy of antifreeze protein types in protecting liposome membrane integrity depends on phospholipid class. *Biochim. Biophys. Acta* **1524**, 11–16 (2000)
126. Knight, C.A., Driggers, E., Devries, A.L.: Adsorption to ice of fish antifreeze glycopeptide-7 and glycopeptide-8. *Biophys. J.* **64**, 252–259 (1993)
127. Franks, F., Morris, E.R.: Blood glycoprotein from Antarctic fish. Possible conformational origins of antifreeze activity. *Biochem. Biophys. Acta* **540**, 346–356 (1978)
128. Tomczak, M.M., Hinch, D.K., Estrada, S.D., Wolters, W.F., Crowe, L.M., Feeney, R.E., Tablin, F., Crowe, J.H.: A mechanism for stabilization of membranes at low temperatures by an antifreeze protein. *Biophys. J.* **82**, 874–881 (2002)
129. Tomczak, M.A.C.: In: Ewart, K.V., Hew, C.L. (eds.) *Fish Antifreeze Proteins*. World Scientific Publishing, Singapore, pp. 187–212 (2002)
130. Tomczak, M.M., Hinch, D.K., Crowe, J.H., Harding, M.M., Haymet, A.D.J., Ward, L.G., Harding, M.M.: The effect of hydrophobic analogues of the type I winter flounder antifreeze protein on lipid bilayers. *FEBS Lett.* **551**, 13–19 (2003)
131. Haymet, A.D.J., Ward, L.G., Harding, M.M.: winter flounder antifreeze proteins: synthesis and ice growth inhibition of analogues that probe the relative importance of hydrophobic and hydrogen bonding interactions. *J. Am. Chem. Soc.* **121**, 941–948 (1999)
132. Hartel, R.W.: *Crystallization in Foods*. Aspen, Gaithersburg (2001)

133. Li, B., Sun, D.-W.: Novel method for rapid freezing and thawing of foods—a review. *J. Food Eng.* **54**, 175–182 (2002)
134. Warren, G.J., Mueller, G.M., McKown, R.L.: Ice crystal growth suppression polypeptides and method of making. US Patent (1992)
135. Payne, S.R., Sandford, D., Harris, A., Young, O.A.: The effects of antifreeze proteins on chilled and frozen meats. *Meat Sci.* **37**, 429–438 (1994)
136. Payne, S.R., Young, O.A.: Effects of pre-slaughter administration of antifreeze proteins on frozen meat quality. *Meat Sci.* **41**, 147–155 (1995)
137. Boonsupthip, W., Lee, T.-C.: Application of antifreeze protein for food preservation: effect of type III antifreeze protein for preservation of gel forming of frozen and chilled actomyosin. *Food Sci.* **68**, 1804–1809 (2003)
138. Aldred, D.L., Berry, M.J., Cebula, D.J., Cox, A.R., Golding, M.D., Golding, S., Keenan, R.D., Malone, M.E., Twigg, S.: Frozen products. US Patent (2006)
139. Sun, D.-W., Zheng, L.: Innovations in freezing process. In: Sun, D.-W. (ed.) *Handbook of Frozen Food Processing and Packaging*, pp. 175–195. CRC Press, Boca Raton (2006)
140. Tachibana, Y., Fletcher, G.L., Fujitani, N., Tsuda, S., Monde, K., Nishimura, S.: Antifreeze glycoproteins: elucidation of the structural motifs that are essential for antifreeze activity. *Angew. Chem. Int. Ed.* **43**, 856–862 (2004)
141. Tsuda, T., Nishimura, S.I.: Synthesis of an antifreeze glycoprotein analogue: Efficient preparation of sequential glycopolymers. *Chem. Commun.* **24**, 2779–2780 (1996)
142. Harding, M.M., Garner, J.: Design and synthesis of antifreeze glycoproteins and mimics. *ChemBioChem* **11**, 2489–2498 (2010)
143. Tachibana, Y., Matsubara, N., Nakajima, F., Tsuda, T., Tsuda, S., Monde, K., Nishimura, S.-I.: Efficient and versatile synthesis of mucin-like glycoprotein mimics. *Tetrahedron* **58**, 10213–10224 (2002)
144. Wierzbicki, A., Dalal, P., Cheatham III, T.E., Knickelbein, J.E., Haymet, A.D.J., Madura, J.D.: Antifreeze proteins at the ice/water interface: three calculated discriminating properties for orientation of type I proteins. *Biophys. J.* **93**, 1442–1451 (2007)
145. Harding, M.M., Ward, L.G., Haymet, A.D.J.: Type I 'antifreeze' proteins. Structure-activity studies and mechanisms of ice growth inhibition. *Eur. J. Biochem.* **264**, 653–665 (1999)
146. Nguyen, D.H., Colvin, M.E., Yeh, Y., Feeney, R.E., Fink, W.H.: The dynamics, structure, and conformational free energy of proline-containing antifreeze glycoprotein. *Biophys. J.* **82**, 2892–2905 (2002)
147. Corzana, F., Busto, J.H., Jimenez-Oses, G., Garcia de Luis, M., Asensio, J.L., Jimenez-Barbero, J., Peregrina, J.M., Avenoza, A.: Serine versus threonine glycosylation: the methyl group causes a drastic alteration on the carbohydrate orientation and on the surrounding water shell. *J. Am. Chem. Soc.* **129**, 9458–9467 (2007)
148. Uda, Y., Zepeda, S., Kaneko, F., Matsuura, Y., Furukawa, Y.: Adsorption-induced conformational changes of antifreeze glycoproteins at the ice/water interface. *J. Phys. Chem. B* **111**, 14355–14361 (2007)
149. Sarno, D.M., Murphy, A.V., DiVirgilio, E.S., Jones Jr., W.E., Ben, R.N.: Direct observation of antifreeze glycoprotein-fraction 8 on hydrophobic and hydrophilic interfaces using atomic force microscopy. *Langmuir* **19**, 4740–4744 (2003)
150. Younes-Metzler, O., Ben, R.N., Giorgi, J.B.: Pattern formation of antifreeze glycoproteins via solvent evaporation. *Langmuir* **23**, 11355–11359 (2007)
151. Cui, Y., Turner, G., Roy, U.N., Guo, M., Pan, Z., Morgan, S., Burger, A., Yeh, Y.: Raman spectroscopy shows antifreeze glycoproteins interact with highly oriented pyrolytic graphite. *J. Raman Spectrosc.* **36**, 1113–1117 (2005)
152. Pan, Z., Morgan, S.H., Ueda, A., Mu, R., Cui, Y., Guo, M., Burger, A., Yeh, Y.: Surface-enhanced Raman probing of biomolecules using Ag-coated porous glass-ceramic substrates. *J. Raman Spectrosc.* **36**, 1082–1087 (2005)
153. Hederos, M., Konradsson, P., Borgh, A., Liedberg, B.: Mimicking the properties of antifreeze glycoproteins: synthesis and characterization of a model system for ice nucleation and antifreeze studies. *J. Phys. Chem. B* **109**, 15849–15859 (2005)



154. Garner, J., Harding, M.M.: Design and synthesis of alpha-helical peptides and mimetics. *Org. Biomol. Chem.* **5**, 3577–3585 (2007)
155. Wierzbicki, A., Knight, C.A., Rutland, T.J., Muccio, D.D., Pybus, B.S., Sikes, C.S.: Structure-function relationship in the antifreeze activity of synthetic alanine-lysine antifreeze polypeptides. *Biomacromolecules* **1**, 268–274 (2000)
156. Zwiig, T., Cucarella, V., Kauffeld, M.: Novel biomimetically based ice-nucleating coatings. *Int. J. Mater. Res.* **98**, 597–602 (2007)
157. Solga, A., Cerman, Z., Striffler, B.F., Spaeth, M., Barthlott, W.: The dream of staying clean: lotus and biomimetic surfaces. *Bioinspir. Biomim.* **2**, 126–134 (2007)
158. Grunwald, I., Rischka, K.: Prevention of ice adhesion and ice growth on surfaces: one problem, two prospective solutions. Annual report 2007/08, Fraunhofer IFAM, pp. 66–68 (2008)

Bioinspiration

From Nano to Micro Scales

Liu, X.Y. (Ed.)

2012, IX, 387 p., Hardcover

ISBN: 978-1-4614-5303-1